Jimma University

Jimma Institute of Technology

School of Biomedical Engineering

Biomedical Imaging Program

Image-based skin diseases diagnosis using deep learning

A thesis submitted to the School of Graduate Studies of Jimma Institute of Technology in partial fulfillment of the requirements for the Degree of Master of Science in Biomedical Engineering (Biomedical Imaging)

By

Kedir Ali

Advisor: Gizeaddis L. Simegn (Ph.D.)

Co-advisor: Mr. Kokeb Dese (M.Sc.)

Jan 2022

Jimma, Ethiopia

Declaration

I declare this thesis entitled "***Image-based skin diseases diagnosis using deep learning"*** is my original work and that has not been presented for a degree in any other university.

Done By:

Mr. Kedir Ali	_____	_____
	Signature	Date

Approved By:

Dr. Gizeaddis L. Simegn	_____	_____
	Signature	Date
Mr. Kokeb Dese	_____	_____
	Signature	Date

Examiners:

Million Meshesha (PhD)		January 13, 2022
External Examiner Name	Signature	Date
_____	_____	_____
Internal Examiner Name	Signature	Date
_____	_____	_____
Chair Name	Signature	Date

Acknowledgment

First, I would like to thank Allah for helping me in my life. I also extend my heartfelt gratitude to my Advisors Dr. Gizeaddis Lamesgin and Mr. Kokeb Dese for their effort in advising, supporting, and sharing experience for me to do this work properly. Moreover, my deepest gratitude will be going to my clinical collaborator Dr. Tadele Molla and Mr. Feleke Tilahun for their support in data collection and labeling.

Finally, I want to express my gratitude to all BME staff of Jimma University Medical Center, Eng. Yilma Kitaba, Mr. Mohammed Aliy, Fetulhak Abdurrahman, and all my friends for their support during the research time.

.

Abstract

Skin diseases are the fourth most common cause of human illness that results in enormous non-fatal burden in daily life activities. There are more than 3000 known skin diseases that are caused by chemical, physical and biological factors. Visual assessment in combination with clinical information is the common diagnostic procedure for skin diseases. However, these procedures are manual and require experience and excellent visual perception. Even though there are sophisticated imaging devices in the market which provide better diagnosis results, their cost limits affordability in a low-resource setting.

Different Artificial intelligence-based computer-aided diagnosis systems have been proposed in the literature to diagnose skin disease from clinical images. However, most of them were based on the availability of online datasets rather than the prevalence of diseases, mainly concentrated on the diagnosis of skin tumors and cancers, and accuracy needs to be further improved.

In this study, an automated system is proposed for the diagnosis of five common skin diseases using data from clinical images and patient information based on the pre-trained mobilenet-v2 model. Clinical images were acquired using different smartphone cameras and patient information was collected during patient registration. Shades of gray color constancy algorithm were applied to remove the color cast resulting from different illumination sources. The training images were rotated by 90°, flipped horizontally and vertically to increase the size of the training set. Multi-class classification accuracy of 87.9% has been achieved using a multiclass classifier using the clinical images only. Integrating patient information with clinical images improve the multiclass classification by 9.6%, resulting in an overall accuracy of 97.5%.

A smartphone android application has been developed for ease of use for the proposed skin disease diagnosis system. The proposed system can be used as a decision support system in low resource setting where both expert dermatologists and the means are limited. Even though the proposed work achieved the best performance, further improvement is required by expanding the size of the dataset, including other common skin diseases.

Keywords: Skin Disease Diagnosis; Image Processing; Deep Learning; Combining Patient Information with Clinical Image Features

Table of Contents

List of figures

List of tables

Acronyms and Abbreviations

AD – Atopic Dermatitis

AV – Acne Vulgaris

AI – Artificial Intelligence

ANN – Artificial Neural Network

CAD – Computer-Aided Diagnosis

CM – Confusion Matrix

CNN – Convolutional Neural Network

DCNN - Deep Convolutional Neural Network

DL - Deep Learning

ISIC – International Skin Imaging Collaboration

LP – Lichen Planus

ML - Machine Learning

OCH – Onychomycosis

ROC - Receiver Operating Characteristic curve

SVM - Support Vector Machine

TCA – Tinea Capitis

Chapter 1

Introduction

1.1. Background of the study

Skin is the largest organ of the body which provides protection, regulates the body fluids and temperature, and enables a sense of the external environment [1]. Skin diseases are the most common cause of all human illnesses which affects almost 900 million people in the world at any time [2]. According to the Global Burden of Disease project, skin disease is the fourth leading cause of nonfatal disease burden throughout the world [3]. An estimated 21 – 87 % of children in Africa are affected by skin diseases [4]. This is due to mechanical, physical, chemical, and biological factors. Moreover, the diseases are given less attention compared to other serious diseases because of their low mortality. However, the overall morbidity causes a financial burden to the community and place a strain on health professionals.

There are more than 3000 known skin diseases worldwide [5]. Acne vulgaris, atopic dermatitis, lichen planus, onychomycosis, and tinea capitis are among the common skin diseases. Some statistics show that atopic dermatitis affects 20% of children below the age of two [6]. The global prevalence of onychomycosis is 5.5 % and contributes 50% of all nail diseases [7]. Moreover, in Ethiopia, 32.3% of school-aged children suffer from tinea capitis [8]. Therefore, skin diseases cause strain to health professionals and financial, socio-economic, and psychological burden to society.

The common procedures for diagnosing skin diseases are patient history and symptom analysis, skin scraping, visual inspection, dermoscopic examination, and skin biopsy. However, those diagnosis methods are tedious, time-consuming, and prone to subjective diagnosis because it requires experience and excellent visual perception. Currently, there is sophisticated and robust medical imaging equipment available in the market. However, the procedures are complex, expensive, and limited to centralized health institutions.

Nowadays, computer-aided diagnosis introduced and reduces the burden for health care professionals with the help of artificial intelligence. Following the emergence of sophisticated technologies, different researchers [9–22] tried to find the best way to diagnose skin diseases.

However, Most works focused on the diagnosis of tumor and cancer [9–12], [15], [17], [19–22], diseases that occur in a specific part of the body [22], didn't consider a symptom of the diseases [9–12], [20–22] that can provide significant information for differentiating skin diseases, and the reported accuracy needs to be further improved.

This study focused on the diagnosis of the five common inflammatory and fungal skin conditions by combining clinical images acquired using a smartphone camera with patient information. This automated diagnosis tool was developed by using a pre-trained mobilenet-v2 model and deployed on a smartphone for ease of use.

1.2. The motivation of the study

Recently, the advent of medical technology enables robust diagnosis of disease in the health sector. Specifically, there are sophisticated imaging technologies that enable to get medical images for accurate diagnosis of diseases. However, these technologies are limited to a centralized health care institution. There is a limited number of dermatologists in developing countries like Ethiopia who actively serve the population. However, people who live in rural areas do have not access to dermatological care services. Nowadays, the ubiquitousness of smartphones capable of capturing a high-quality image, large storage capacity, and high-performance processor give promise in the health sector. Therefore, we are motivated to propose smartphone-based skin diseases diagnosing system that can reduce a burden for an expert dermatologist, enables the diagnosis of the diseases in a rural area, and self-assessment of disease which reduces unnecessary expense. Moreover, most research proposed so far is mainly concentrated on the diagnosis of skin cancer. In developing countries, inflammatory skin conditions, infection, and infestation are common [4]. Therefore, we concentrated to propose a system capable of diagnosing inflammatory skin conditions.

1.3. Statement of the problem

Skin diseases are the most common cause of all human illnesses [2]. The common procedures for diagnosing skin diseases are patient history and symptoms analysis, skin scraping, visual inspection, dermoscopic examination, and skin biopsy. However, those diagnosis methods are tedious, time-consuming (average 40 minutes), and prone to subjective diagnosis. Most of them require experience and excellent visual perception. There are sophisticated and robust medical imaging modalities available in the market. However, the cost of the equipment limits the affordability in a low-resource setting.

Computer-aided diagnosis systems can improve diagnostic accuracy and reduce the subjective judgment of the disease categories. There are more than 3000 skin diseases worldwide that vary due to different factors including environmental factors, hygienic standards, social customs, and genetics. A lot of researches [9–22] were conducted to automatically diagnosis skin diseases that are prevalent in their respective region with promising result. Esfahani *et al.*, Fujisawa *et al.*, Han *et al.*, Mendes *et al.*, and Wu *et al*. proposed a way to diagnose skin tumors including melanoma, basal cell carcinoma, and squamous cell carcinoma. Moreover, Hameed *et al.* proposed an automatic system for the diagnosis of acne, eczema, psoriasis, melanoma, and benign lesion.

However, inflammatory skin diseases are not common as skin cancer in developed countries but are big issues in our community. The skin color of our community is different from the white skin population and most repositories were from the white-skinned community. Therefore, developing an automated system on the white skin dataset and applying it to a fair-skinned population is not the right way. Using images from different images sources was proposed by many researchers. Therefore, this study aims to automate skin diseases diagnosis using image processing and deep learning.

1.4. Research questions

- What are the common skin diseases in southwest Ethiopia?
- How can we prepare a dataset of skin disease and combine image features with corresponding patient information?
- How can we develop a lightweight deep learning model with high accuracy and suitable to deploy on a smartphone?

1.5. Objective of the study

1.5.1. General objective

The general objective of this study is to develop an automated prototype for the diagnosis of five skin diseases using deep learning from combined clinical image features and patient information.

1.5.2. Specific objectives

The specific objectives are:

- To study the pattern of skin diseases in Southwest Ethiopia
- To collect and prepare a clinical image dataset with the corresponding patient information.
- To develop automatic skin diseases diagnostic system with high accuracy using the state-of-the-art and lightweight deep learning model.

1.6. Significance of the study

Skin diseases are the fourth most common cause of human illness that results in an enormous non-fatal burden throughout the world [3]. This is because of the lack of High-Tec diagnostic devices, cost of the diagnosis, poor health awareness, and a limited number of dermatologists.

This study enables the diagnosis of five skin diseases with better accuracy and less duration of time. It is important to diagnose the disease in rural areas where expert dermatologist is not available, assist general practitioners, regional and rural practitioners, and self-assessment for patients. Moreover, the future researcher can use our dataset for further investigation and the result of preliminary investigation of the pattern of skin diseases also gives significant information on the prevalence of skin diseases.

1.7. Scope and limitation of the study

This study investigated the prevalence of skin diseases in southwest Ethiopia and proposed a lightweight deep learning model for the diagnosis of five diseases namely, acne vulgaris, atopic, dermatitis, lichen planus, onychomycosis, and tinea capitis. Shades of gray color constancy algorithm were applied for effective removal of color casts. It followed hierarchical approaches for the diagnosis of the skin condition, the input image is classified as healthy or abnormal using the binary classifier model. If the output of the binary classifier was abnormal, the multiclass classifier classifies the given image into five skin conditions or as unknown if the result does not belong to the five categories.

The proposed work gave a promising result for the diagnosis of five skin diseases and provide relevant information regarding the prevalence of skin disease. However, the preliminary investigation conducted for a pattern of skin diseases was limited to southwest Ethiopia. Investigating the pattern of skin diseases at the national level enables for effective handling of skin diseases. The dataset collected mainly includes a fairly-skinned population and did not include black-skinned populations like Gambella and Benishangul. Collecting image datasets from those populations makes the model robust and suitable to implement in all regions of the country. Moreover, there are a lot of common skin diseases that did not include in this study due to lack of time and money.

Chapter 2

Literature review and related works

2.1. Human skin

Skin is the largest organ of the body that provides protection, regulates body fluids and temperature, and enables sensing of the external environment [1]. The skin is composed of the outermost layer called the epidermis, the middle layer dermis, and subcutaneous tissue as shown in *Figure 2.1*. The epidermis consists of a group of cells known as keratinocytes, which function to synthesize keratin, with a protective role. The epidermis is connected to the dermis by interlocking its epidermal ridges or pegs with dermal papillae and it has no blood cells. The dermis lies between the outermost layer epidermis and subcutaneous tissue. It is made up of the fibrillar structural protein known as collagen and provides structural and nutritional support for the epidermis. The subcutaneous tissue contains small lobes of fat cells known as lipocytes [23].

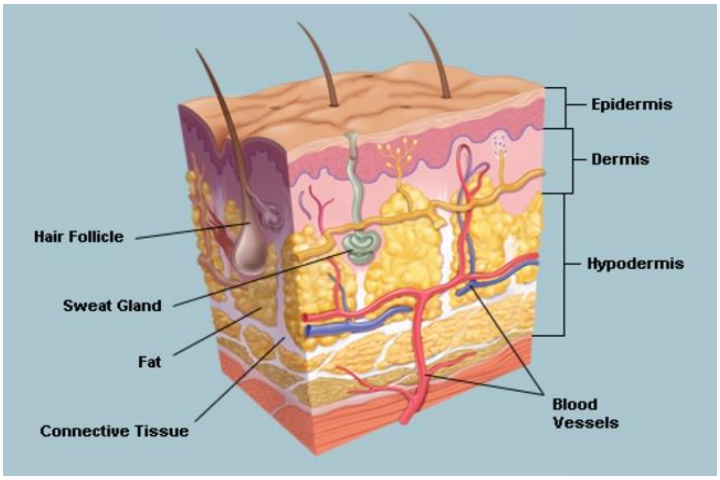

Figure 2.1: Anatomy of human skin [24]

2.2. Skin diseases

Skin diseases are any condition or disorder, that can affect human skin and can be temporary or permanent. It is the most common cause of all human illnesses which affects almost 900 million people in the world at any time [2]. According to the global burden of disease project, skin disease is the fourth leading cause of nonfatal disease burden throughout the world [3]. An estimated 21 – 87 % of children in Africa are affected by skin diseases [4]. This is due to mechanical, physical, chemical, and biological factors [25]. Skin diseases are given less attention compared to other

serious diseases because of their low mortality. However, the overall morbidity causes a financial burden to the community and places a strain on health professionals. It can cause pain and spoil the appearance of the patient's skin. It results in diverse effects in life including education, relationships, self-esteem, career choices, social, sexual, and leisure activities. Patients with some skin diseases have a higher potential for anxiety, depression, and suicidal ideation [26].

There are more than 3000 known skin diseases worldwide [5]. In developing countries, infection, and infestation are more common [4]. This study focused on the diagnosis of five common skin problems: acne vulgaris, atopic dermatitis, lichen planus, tinea capitis, and onychomycosis. The criteria for diseases selection were the result of the preliminary study and the occurrence of the diseases throughout the data collection period.

2.2.1. Acne vulgaris

Acne vulgaris (Vulgaris is a Latin word meaning common) is a chronic inflammatory disease of the pilosebaceous unit. It is characterized by seborrhea or excess grease, inflammatory and non-inflammatory lesions, and scars [27]. It usually invades the face (see Figure *2.2*), neck, anterior and posterior torso. Abnormal follicular keratinocyte hyperproliferation, increased sebum production, the proliferation of microorganisms and inflammations are the main factors contributing to the development of acne [28]. Acne distresses the self-esteem, mood and, psychology of individuals[28, 29].

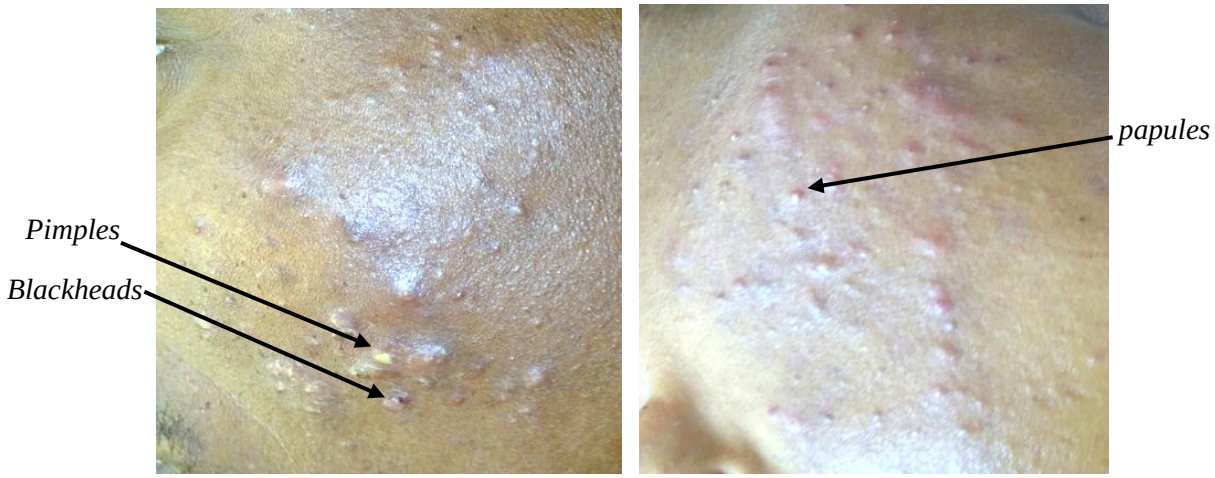

Figure 2.2: Acne vulgaris on the lateral face

2.2.2. Atopic dermatitis

Atopic dermatitis (Atopic eczema) is a chronic inflammatory disease that affects the wellbeing of a patient's life. It is the first step of the atopic march (the progression of atopic manifestation) later results in other allergic disorders like Asthma. It damages the skin barrier and increases the loss of water resulting in dry, itchy skin infection and increase skin allergy. It affects 20% of children below the age of two-year-old [6]. It mainly appears on the face (Figure *2.3* - a), creases of the elbow, back of the knee, neck, anterior torso (Figure *2.3*- b), wrists, back, shoulder, and ankles in older children and adults. Atopic dermatitis has a social, economic, occupational, and psychological impact on society [30].

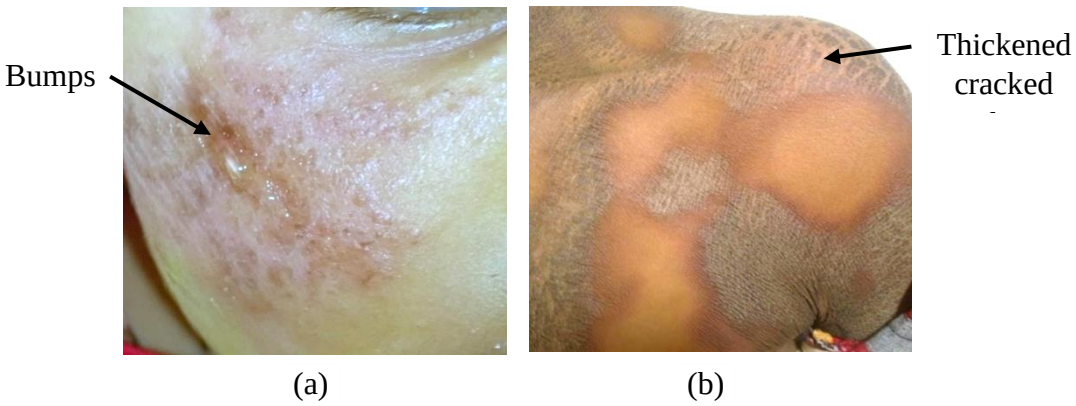

Figure 2.3: Atopic Dermatitis in a different region of the body

2.2.3. Lichen planus

Lichen planus is a chronic inflammatory mucocutaneous disease that affects the skin, hair, nail, and mucosae. It mainly presents in the middle-aged adult and elderly population [31, 32]. Cutaneous lichen planus commonly appears on the flexor surface and limbs. Hyperpigmentation (Figure *2.4*) and itching are the major burdens to a patient with lichen planus, which affects the wellbeing of society.

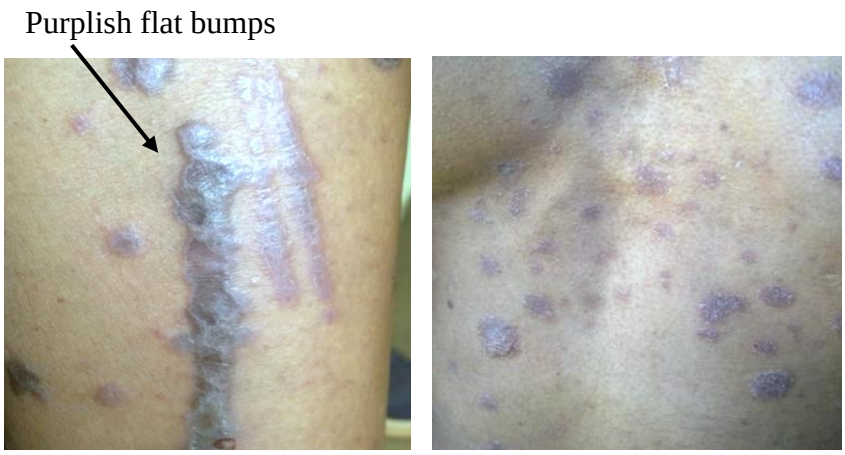

Figure 2.4: Lichen planus on the lower extremity (left) and anterior torso (right)

2.2.4. Onychomycosis

Onychomycosis is the most common fungal nail disorder in the world. This fungal infection is caused by a dermatophyte (pathogenic fungus on the skin), non-dermatophyte molds, and yeasts. It highly influences the quality of life of individuals. Onychomycosis is less common in children and the prevalence increases with age [33, 34]. The global prevalence of onychomycosis is around 5.5% and contributes 50% of all nail diseases [33]. The risk factors are trauma, pathogenic fungi, poor peripheral circulation, and poor hygiene. Figure *2.5* shows fungal nail infection on the finger and nail tips.

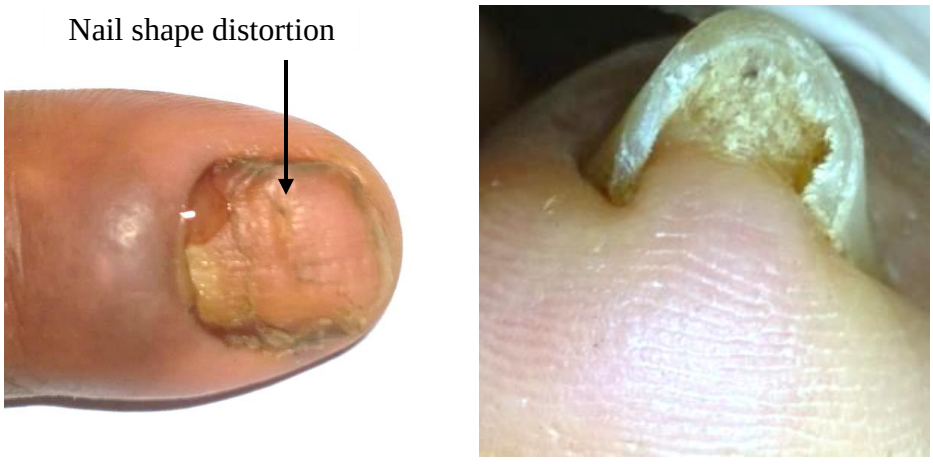

Figure 2.5: Fungal nail infection

2.2.5. Tinea capitis

Tinea capitis (ringworm of the scalp) is the most common superficial cutaneous fungal infection of the scalp caused by dermatophytes [35]. The invasion of dermatophytes results in hair loss, scaling, black dot, and erythema. It is more prevalent in children between three and seven years of age [36]. The total estimated cases of tinea capitis in Africa children were 138.1 million. Nigeria contributes 16.4% and Ethiopia contributes 8.5% of the total cases [37]. The poor habit of personal hygiene, poor environmental sanitation, and regular contact between children plays a great role in the susceptibility of the disease. Sample images of tinea capitis are shown in Figure *2.6.*

Figure 2.6: Tinea capitis (ringworm of the scalp)

2.3. Diagnosis of skin diseases

2.3.1. Patient history and symptom

History of present skin condition such as; duration, site of onset, details of spread and enlargement of the lesion, and provoking or aggravating factors and symptoms (itchy, odor, pain) provides significant information for diagnosis. Furthermore, history of skin disorder, past and present general medical, family, social history and medication used to treat present skin condition are responsible for effective diagnosis of skin diseases.

2.3.2. Skin scrapping

Scales are removed by gentle scraping of the skin by using a scalpel blade and treated with potassium hydroxide to remove keratin and other obscuring debris. The treated skin scale will be examined using a microscope.

2.3.3. Visual Inspection

Skin diseases are visible with the naked eye and the lesion can be touched and palpated. However, it is necessary to know what to look for and understand what is seen and felt. The distribution, symmetry, size, morphology, and shape of the lesion help to diagnose skin diseases appropriately.

2.3.4. Dermoscopic examination

Dermoscopy (epiluminescence microscopy, dermatoscopy, amplified surface microscopy) is a useful tool for early melanoma recognition and differential diagnosis of pigmented skin lesions. Depending on the type of lesion and experience of the physician, dermatoscopy can increase the accuracy of diagnosis.

2.3.5. Skin biopsy

Skin biopsy is used to evaluate skin lesions when clinical uncertainty occurs during an investigation. This standard procedure is performed by taking skin samples and examining to obtain information about the medical condition of the skin. It is a gold standard for confirming uncertainty in skin lesion diagnosis.

2.4. The drawback of the conventional diagnostic system

The main routine diagnostic system for skin diseases in low-income countries is visual examination, laboratory testing, patient history, biopsy, and using dermoscopy. Even though there are a limited number of dermatologists and general practitioners, they are actively serving society to reduce the burden of skin disease. However, the above techniques are tedious, time-consuming, and lead to a subjective diagnosis.

2.5. Imaging technologies

The advent of advanced imaging technologies in the health sector has recently shown promise in providing robust diagnosis and optimal treatment of diseases. Digital photographic imaging, confocal microscopy, optical coherence tomography, high-frequency ultrasound, dermatoscopy, fluorescent imaging, and Raman spectroscopy are the most recent imaging technologies [38].

However, these techniques are complex, expensive, and limited to centralized healthcare facilities that leave low resource setting populations without access to dermatological services.

Nowadays, smartphone-based imaging and sensing platforms have become an alternative for filling the gaps. The latest generation of a smartphone with a high-definition camera, large storage capacity, and high-performance processor enables to capture of digital images and record videos with better resolution [39]. Portability, cost-effectiveness, and connectivity make a smartphone to be applicable in many areas [40, 41]. The availability of smartphones equipped with digital cameras enables the acquisition of clinical images for investigation using computer-aided diagnosis (CAD).

2.6. Computer-aided diagnosis of Skin Diseases

Computer-aided diagnosis (CAD) is a system that can help doctors to interpret medical images. It provides important information to analyze and evaluate tasks requiring professional expertise. It provides cost-effective and objective judgment within a short time. Automated computer-aided diagnosis systems for the diagnosis of skin diseases are designed using artificial intelligence.

2.6.1. Artificial intelligence

Artificial intelligence (AI) is the development of a computer system or a machine that can perform tasks that requires human intelligence. Some of these tasks include; visual perception, speech recognition, decision-making, and language translation. The categories and subcategories of artificial intelligence are machine learning, deep learning, cognitive computing, computer vision, and natural language processing [42]. AI in health care sectors is used to support clinical decisions**,** enhance primary care and triage through chatbots**,** robotic surgeries**,** virtual nursing assistants, and aid in the accurate diagnosis of diseases. The widespread acknowledgment of artificial intelligence and medical imaging paves the way for objective judgment of diseases diagnosis [43, 44].

2.6.1.1. Machine Learning

Machine learning (ML) is a subset of artificial intelligence which involves the development and deployment of algorithms for completing a predetermined task. This data-driven algorithm mimics human behavior based on prior experience without explicitly being programmed [45]. The workflow of machine learning algorithms in medical imaging includes taking medical images as input, segment area of interest, manual extraction of representative features, selecting best image features, discarding noise, and classification. Machine learning models take the given data

(handcrafted features) and learn through trial and error to predict the answer from the inputted dataset [46]. The main categories of machine learning algorithms are supervised, semi-supervised, unsupervised, reinforcement, and active learning [47]. Machine learning algorithms are applied in different areas of medical imaging including 3D breast and lesion segmentation and classification [48], and segmentation and classification of skin disease [12].

2.6.1.2. Deep Learning

Deep learning (DL) is a subset of machine learning that can extract meaningful and discriminative features by analyzing huge data [49]. Artificial neural networks are a basis for deep learning algorithms and perform tasks by mimicking how a human brain works [50]. An artificial neural network consists of several neurons that can perform a mathematical operation on inputs fed to the neurons. All inputs are multiplied by their corresponding weight. The output of each neuron is also multiplied by its weight and the process continues in all neurons in the network. The outputs of the last layer are fed to the output neurons. The weights of each neuron are updated using backpropagation. Multiple layers are interconnected between the input and output layers to form a deep neural network. Figure 2.7 demonstrates the schematic representation of a simple artificial neural network.

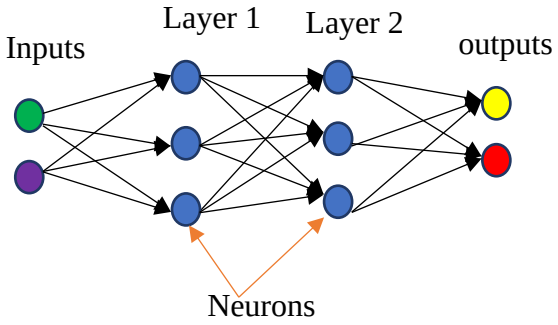

Figure 2.7: Schematic representation of an artificial neural network

A convolutional neural network (CNN) is a subtype of artificial neural network which is suitable for image analysis [47]. This common method of deep learning comprises convolutional, pooling, activation, and fully connected layers [51]. The convolutional layers extract meaningful image features using several convolutional filters. The pooling layer reduces the output feature maps and the activation layer introduces non-linearity to the network. Fully connected layers are used to

reduce the dimension of the output feature map and as a classifier. The schematic representation of the convolutional neural network is shown in Figure *2.8*.

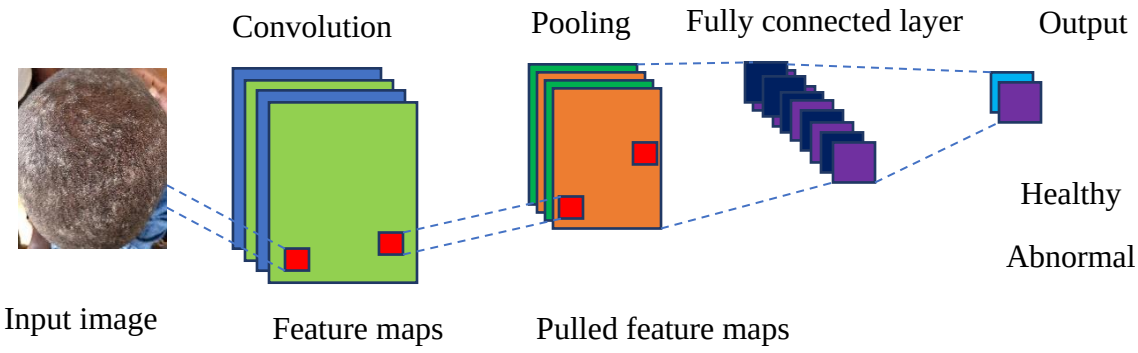

Figure 2.8: Schematic diagram of simple convolutional neural network

2.6.1.3. Transfer learning

Transfer learning is a way of repurposing a pre-trained model on a related problem domain by passing a weight of the trained model to a new neural network. Pretrained models are deep learning models trained on the specific problem domain. Pretrained models are quite competitive when compared to training from scratch with less computational power and time [52]. There are a lot of pre-trained models for image recognition trained on the ImageNet dataset including AlexNet, VGG-19, ResNet-10, and ResNet-50 [53]. Those models can be used as either fixed feature extractors or as a classifier by freezing the convolutional base of the trained model.

2.7. Related works on automatic skin diseases classification

Different kinds of literature have proposed a means of diagnosing skin diseases using clinical images [9–22]. Most of them apply a conventional machine learning approach and deep learning techniques to construct a model for skin diseases diagnosis from clinical images.

Support vector machine (SVM) with quadratic kernel has been proposed in [12], for the classification of acne, eczema, psoriasis, benign and malignant melanoma. They resized all images to 720x720 pixels to make a consistent in size. Noise in the form of hair is removed using a Dull Razor algorithm and the image was smoothed using a gaussian filter. The proposed work achieved an accuracy of 83%. However, they did not apply an efficient preprocessing algorithm to reduce the color variation of clinical images acquired using different devices. This work is mainly proposed on an available online public database of white skin. Moreover, they did not apply deep learning techniques that can further boost the overall classification accuracy.

Different literature has proposed the classification of skin tumors using transfer learning techniques [14,15], [17–19]. Research reported in [15] used a convolutional neural network as a deep learning framework for classifying melanoma and benign lesion. To improve the classification accuracy of the model illumination correction was performed. Moreover, data augmentation techniques such as cropping, scaling, and ration were applied to increase the training set and they claimed an accuracy of 81%. Additionally, a multi-class classification system was proposed using ResNet152 for 12 skin diseases [17, 18]. Transfer learning and different data augmentation techniques including rotation, random zoom, horizontal and vertical flip, and light variance were applied to handle data scarcity. The overall accuracy of 78% was achieved using the proposed deep learning model [14]. Similarly, Han et al. [13] claimed an area under the receiver operating curve (AUC) of 0.96, 0.83, 0.82, 0.96 for basal cell carcinoma, squamous cell carcinoma, interepithelial carcinoma, and malignant melanoma respectively. A pre-trained GoogLeNet was proposed to classify 14 categories of skin tumors [11]. Five-fold cross-validation was performed to verify the robustness of the proposed model. The performance of the proposed model was compared and surpasses board-certified dermatologists. They claimed an overall accuracy of 76.5%. Recently, Wu et al. [22] compared five pre-trained deep learning frameworks for the diagnosis of six facial skin conditions from a clinical image. They applied different weights in the cost function of different diseases to mitigate data imbalance. Pretrained

inceptionResNet_V2 model achieves a precision of 77% on the diagnosis of Seborrheic keratosis, Actinic keratosis, Rosacea, lupus erythematosus, Basal cell carcinoma, and Squamous cell carcinoma. The proposed works mainly focused on the diagnosis of skin tumors. They claimed low accuracy diagnostic system developed on white-skinned clinical images. The developed system cannot be used as a decision support system for the fair-skinned population. Moreover, they did not integrate patient information that can improve the accuracy of the decision support system.

Velasco *et al. [21]* applied a pre-trained MobileNet model to classify psoriasis, acne, vitiligo, pityriasis rosea, chickenpox, eczema, and tinea corporis. They claimed 94.4% accuracy by using oversampling and data augmentation techniques. The developed model was deployed on a smartphone. Despite the promising result, the developed model did not use patient information that can further boost the diagnosis performance of the proposed system.

Fusion of image and anamnestic data for the classification of benign and malignant melanoma was proposed in [9]. They design a CNN architecture called LesionNet for extracting image features and a fully connected multilayer perceptron called MetaNet for extracting patient information. The output of the two networks was fed to MergeNet that combines the two inputs and fed to the classifier. They claimed an overall accuracy of 88.34% by combing image and patient data features for binary classification of benign and malignant melanoma. Similarly, the effect of incorporating patient information for binary classification of benign and malignant melanoma was investigated by Ruiz-Castilla and Rangel-Cortes [19] and claimed accuracy of 85%. Despite the promising results, the proposed works were limited to the diagnosis of benign and malignant melanoma.

The impact of patient information on the diagnosis of skin cancer was reported in [18]. The proposed work was intended to diagnose six diseases including actinic keratosis, basal cell carcinoma, squamous cell carcinoma, melanoma, nevus, and seborrheic keratosis. Adjusting brightness, contrast, saturation and hue, horizontal and vertical flipping, scaling, zoom, shear was applied to expand the number of the training set. The overall accuracy of 78% was claimed. Moreover, an ensemble of different CNN models for the classification of skin cancer was proposed in [17]. Weight loss function based on labels frequency was applied to tackle class imbalance and efficient preprocessing techniques were used to further boost the performance of the model. The overall accuracy of 91% was achieved. Classification of actinic keratosis, basal cell carcinoma,

benign keratosis, dermatofibroma, melanoma, nevus, and vascular lesion using image and background information of patient was proposed [20]. Pretrained AlexNet was finetuned and an improved accuracy of 80 was achieved. The proposed works showed good results for the diagnosis of skin diseases. However, they mainly focused on the diagnosis of skin cancer while leaving inflammatory skin conditions. The patient information mainly contains age, gender, and anatomical site. Incorporating diseases symptoms also provides a clue for differentiating the diseases.

In summary, the proposed works showed promising results for the diagnosis of different skin diseases from clinical images. However, most of the works were dependent on the availability of an online public dataset, focused on cancer and tumors, and are designed to diagnose specific parts of a body. The datasets collected and used mainly consists of white skin. Moreover, the diagnostic performance, including the accuracy reported is not satisfactory. Table *2-1* shows the summary of the recent studies on the automatic diagnosis of skin diseases using clinical images.

Table 2-1: Summary of the related works

Authors	**Method**	**Diagnosed diseases**	**Result**	**Gap**
Nasr-Esfahani et al. [15]	CNN	Melanoma & Benign Lesion	Accuracy = 81%	• Only diagnose melanoma & benign lesion • Low accuracy • Patient information not included.
Fujisawa et al.[11]	GoogLeNet	Malignant Melanoma, Squamous cell carcinoma, Bowen diseases, Actinic Keratosis, Basal cell carcinoma, Nevus cell nevus, blue nevus, congenital melanocytic nevus, Spitz nevus, sebaceous nevus, poroma, seborrheic keratosis, nevus spills, and lentigo simplex	Accuracy=76.5%	• Inflammatory skin condition not included (only skin tumor and related condition) • Patient information not included. • Low accuracy
Hameed et al.[12]	Decision tree, **SVM**, KNN, ensemble classifier, ANN	Acne, Eczema, Psoriasis, Benign and Malignant melanoma	Accuracy = 83%	• Deep learning can further boost diagnostic performance. • Efficient preprocessing not applied. • Patient information not included.

Han et al.[13]	ResNet152	Malignant melanoma, Basal cell carcinoma, Squamous cell carcinoma, Interepithelial carcinoma, Actinic keratosis. Seborrheic keratosis, Dermatofibroma, Melanocytic Nevus, Hemangioma, Lentigo, Pyogenic granuloma, Wart	**Asan dataset AUC** BCC = 0.96 ± 0.01 SCC = 0.83 ± 0.01 IEC = 0.82 ± 0.02 MM = 0.96 ± 0.00	• Healthy skin image not included (reduce false-positive results) • Patient information not included. • Low accuracy
Mendes et al.[14]	ResNet152	Malignant melanoma, Basal cell carcinoma, Squamous cell carcinoma, Interepithelial carcinoma, Actinic keratosis, Seborrheic keratosis, Dermatofibroma, Melanocytic Nevus, Hemangioma, Lentigo, Pyogenic granuloma, Wart	Accuracy = 78%.	• Patient information not included. • Only focus on skin tumor • Low accuracy
Wu et al.[22]	ResNet50, Inception V3, DenseNet121, Xception, **Inception-Resnet V2**	Seborrheic keratosis, Actinic keratosis, Rosacea, lupus erythematosus, Basal cell carcinoma, and Squamous cell carcinoma	Precision = 77%	• Diagnose only facial skin conditions. • No patient information is included. • Low accuracy

J.Velasco, et al.[21]	MobileNet	Acne, eczema, chicken-pox, pityriasis rosea, psoriasis, tinea corporis, and vitiligo	Accuracy= 94.4%	• Different datasets and diseases • No patient information included • Low accuracy

Chapter 3

Methodology

3.1. Overview

A research methodology is a set of specific procedures or techniques used to identify select and analyze information about a research topic. This section allows the readers of this paper to have a good insight into the specific procedures followed and the work performed to achieve the best performing automated system for skin diseases diagnosis using clinical images and patient information. This research includes literature review, data collection, and labeling, preprocessing, model training and evaluation, model deployment, and refinement. All these procedures are organized and presented in the next section.

3.2. Research design

In this study, experimental research is followed since it is helpful to develop of automatic skin diseases diagnosis system systematically through experiments. Experimental research design enables researchers to manipulate variables. There are independent variables such as the datasets and algorithms and dependent variables including the parameters used and performance evaluation matrices. The general procedure of the proposed work is shown in Figure *3.1*

The dataset includes both clinical images and patient information. Data were split as training and test set. The training set (clinical images and patient information) was used to develop the model. The pre-trained mobilenet-v2 model was used as a feature extractor for clinical images. The output of the mobilenet-v2 model was concatenated with patient information and fed to the classifier. The classifier gets both clinical image features extracted pre-trained mobilenet-v2 model and one hot encoded patient information. Therefore, the model was developed using the pre-trained mobilenet-v2 model as image feature extraction and capable of accepting auxiliary patient information. Patient information was used for the learning process to develop and test the model. The independent test set (clinical images and patient information) was used to evaluate the performance of the model after training was completed. The developed model is deployed on a smartphone for ease of use.

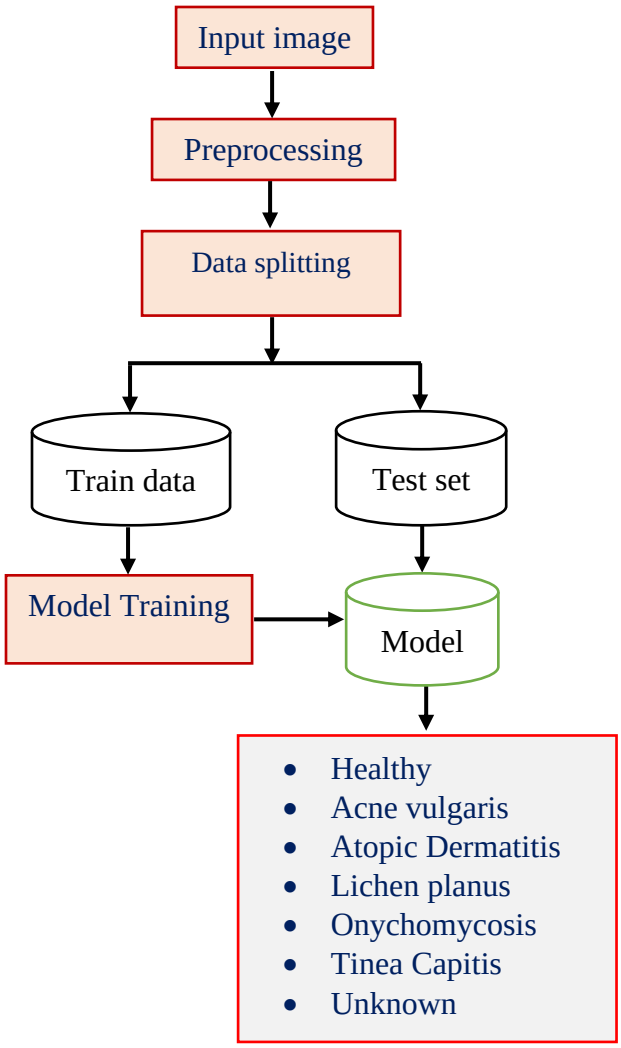

Figure 3.1: Block diagram of the proposed work

3.3. Data collection and preparation

3.3.1. Study area

Dr. Gerbi medium clinic is the most renowned clinic in Jimma and neighboring zones of southwest Ethiopia, that mainly provides dermatological service and other clinical care. Currently, the clinic provides various clinical services by employing specialist doctors, general practitioners, laboratory technicians, nurses, and others. All data about the pattern of skin diseases in southwest Ethiopia from Dr. Gerbi's medium clinic. The clinical images and patient information were taken from both Dr. Gerbi medium clinic and Boru Meda general hospital.

3.3.2. Study population and sampling

The study population for the pattern of skin diseases in southwest Ethiopia was all patients with different skin diseases who attend Dr. Gerbi medium clinic, Jimma, Southwest Ethiopia from August 2019 to April 2020. Patients with different skin conditions were de-identified from the medical record of the clinic.

The non-probability sampling approach was used to determine the pattern of skin diseases. It is cheap, more convenient, and more appropriate for exploratory study. Purposive sampling, also known as selective sampling, is a sampling technique that depends on the researcher's judgment when selecting samples and applied for this study. Patients who visited Dr. Gerbi's dermatological clinic made up the research sample.

3.3.3. Data collection

The clinical and image data were collected from the most renowned dermatological clinic of Dr. Gerbi medium clinic, Jimma, and Boru Meda hospital of Dessie. The main tasks performed in this step were two, identifying the type and number of diseases from the medical record and capturing the clinical image dataset. The disease type and the number of diseases were identified by counting the medical records of the patient. The clinical images were captured after the diagnosis result was confirmed by the expert dermatologists using smartphones having different camera resolutions.

3.3.4. Preprocessing

The clinical images were acquired using different smartphones under different lighting conditions and experiencing different colors. This color cast was corrected by applying the shades of gray color constancy algorithm. The images were resized to have consistent image size and to reduce memory requirements. Patient information was converted to a feature vector using the one-hot encoding technique. The collected dataset was split into 80% training, 10% validation, and 10% test sets.

3.4. Implementation tool selection for prototype development

The proposed models were designed to operate hierarchically, first, the binary classifier classifies the input as healthy or abnormal. If the result of the binary classifier was abnormal the input will feed to a multiclass classifier and return the diagnosis result (acne vulgaris, atopic dermatitis, lichen planus, onychomycosis, and tinea capitis). The state-of-the-art and lightweight pre-trained deep learning model (MobileNet_v2) was selected and fine-tuned to be used as a binary and

multiclass classifier. The model was developed by training using the training dataset and validated using the validation set during the training phase. The learning rate, batch size, and the number of epochs was adjusted to develop the best-performing model.

The developed model was used on a smartphone as an independent application. The application was developed using android studio and was written using a java programming language. The first version of the application was distributed to my friends and an expert dermatologist for feedback. Based on their feedback modification were made on the layout and some functionalities including how to feed patient information. The current version of the application returns the diagnosis result in two languages (Amharic and English).

3.5. Performance evaluation

The performance of the model was evaluated after training using an independent test set. The model's performance was expressed using different evaluation metrics including accuracy, precision, recall, f1-score, kappa score, and receiver operating curve. Accuracy measures the proportion of correct classification, precision measures the proportion of correct positive classification from positive prediction, and recall measures the proportion of correct positive prediction from the actual true. The receiver operator characteristic (ROC) curve is a graph that gives information about how the model correctly classifies positive and negative samples. The kappa value is a metric used to compare an observed accuracy with an expected accuracy or random chance. Moreover, the confusion matrix was also plotted to see the model's prediction for a given test set.

Chapter 4

Methods and algorithms

4.1. The pattern of skin diseases in Southwest Ethiopia

The data used for analyzing the pattern of skin diseases was collected from the most renowned dermatological clinic called Dr. Gerbi medium clinic. Based on a signed letter from the school of biomedical engineering the owner of the hospital grants permission to access data. The required data was taken from the medical record of patients. All skin cases were de-identified by counting the medical record manually. The total number of patients for each disease, age, and gender information was registered. Figure *4.1* demonstrates the identification procedure of diseases from the medical record. Statistical analysis was performed after necessary data registration.

Figure 4.1: Diseases de-identification Procedure

4.2. Data variables and Analysis

The study variables are the patient's age, sex, and diagnosis of the disease. Patients were from different wereda and towns of Jimma zone, Metu, Mizan, Tepi, Naqamte, Addis Ababa, Bonga, Dawro, Gambella, Bedelle, Dembi, Bale, Dimma, and others. The total number of diseases were identified from the medical record of patients. Moreover, the total number of patients per disease, the mean age, and gender information were calculated using a formula in Appendix B. During de-identification procedures, there was missing information (gender). As a result, the summation of male and female attendants may not equal the total number of patients per disease.

4.3. Result and discussion

A total of 119 skin diseases from 8325 patients were de-identified. The total number of male and female patients was identified. Moreover, the mean age of each disease is calculated. The details of the analysis result are demonstrated in Appendix B: Analysis result of the pattern of skin diseases in southwest Ethiopia. The number outside the bracket indicates the total number whereas the number inside the bracket is the percentage of each disease and male and female attendants.

The pattern of skin diseases varies due to ecological factors, hygienic standards, social customs, and genetics. This preliminary study was designed to get information about skin diseases in southwest Ethiopia. The mean age, gender, and diseases type are identified.

The result showed that the common skin diseases were atopic dermatitis (7.21%), scabies (6.31%), tina capitis (6.29%), acne vulgaris (6.09%), vitiligo (5.23%), seborrheic dermatitis (5.08%), lichen-simplex chronicus (5.07%), lichen-planus (3.3%), pyoderma (2.64%), Ecthymia contagiosum (2.26%), papular urticaria (2.34%), pityriasis alba (2.08), acute urticaria (1.97%), melasma (1.93%) and onychomycosis (1.77%).On the other hand, icthiosis, cow-pox, sarcoptes, linear verrulated epidermal nevus, and bursitis are rare skin conditions in southwest Ethiopia.

Papular urticaria, tinea capitis, impetigo, kerion, and epidermal nevus are more common in children (mean age of two to ten). Pyoderma, tinea capitis, cheilitis, psoriasis, lichen-simplex chronicus, and seborrheic melasma were more common in men. On the other hand, acne vulgaris, rosacea, paronychia, onychomycosis, and melasma were common in females.

4.4. Automatic Skin diseases Diagnosis

The preliminary study conducted for this research indicates that atopic dermatitis, acne vulgaris, lichen planus, onychomycosis, and tinea capitis are the common skin problems in southwest Ethiopia. In this study, an automatic diagnosis system has been developed based on a deep learning model for five common skin diseases by combining clinical images acquired using a smartphone camera and patient information. A torchvision pre-trained Mobilenet_v2 model which was previously trained on ImageNet has been used for extracting representative clinical image features. The image features were concatenated with the patient data and fed to the SoftMax classifier.

Figure *4.2* demonstrates the general block diagram of the proposed system. The clinical images and patient information were preprocessed before model training. The model was trained using a training set. The independent test set was used to evaluate the performance of the model.

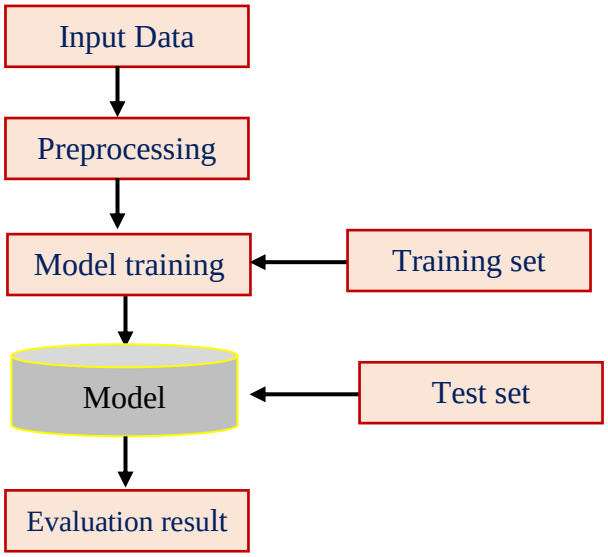

Figure 4.2: Block diagram of the proposed classifier

4.4.1. Data collection

The dataset used for this research was collected from Dr. Gerbi medium clinic of Jimma and Boru-Meda General hospital of Dessie from 268 patients (149 females and 119 males, age range 0-85 years). A total of 1137 images with different resolutions along with patient information was collected from Dr. Gerbi medium clinic and 239 images from Boru-Meda General hospital using a smartphone camera (Nokia window phone, Techno Spark4, SamsungA20, and SamsungJ6). 847 of the images were collected from a healthy subject and 1376 from abnormal skin affected by acne vulgaris, atopic dermatitis, lichen planus, onychomycosis, and tinea capitis disease. The healthy images were all taken from a healthy person. The images were captured after the diagnosis was confirmed by an expert dermato-venereologist and a tropical dermatologist. Moreover, images from other common skin diseases were also included and labeled as an “unknown” class. The unknown class includes 204 images of lichen simplex chronicus, cow pox, monkey pox, leishmania, tinea corporis, rosacea, seborrheic dermatitis, foot ulcer, papular urticaria, discoid lupus erythematosus, onchocerciasis, real-world object images, and others. Table 4-1 shows the number of images collected for each skin disease.

From the collected data, tinea capitis was common in children with the age range of 0-9 years, rare on 10-19 years, and absent above the age of 20 years. On the other hand, atopic dermatitis was found in all age ranges, but it was found to be common within the age range of 0-39. Moreover, acne vulgaris was common in the age range 10-49 years, especially teens and adults were found to be more vulnerable in the age range of 10-29 years. Even though onychomycosis was found to occur evenly in people with the age range 0-59 years, it is more common in the range of 0 -39 years while it is not found above 60 years. In addition, lichen planus was also common between the age of 20-49 and rarely found in teens, adults, and elderly people. This is demonstrated in Figure *4.4*. Figure *4.3* demonstrates gender-wise distribution of skin diseases from the collected data. Acne vulgaris and onychomycosis were common in males than females, and tinea capitis was more common in males than females.

Patient information including age, gender (2, male and female), anatomical sites (17), and symptoms of the diseases (21) were also collected. The anatomical sites include; abdomen anterior torso, armpit, chin, ear, forehead, lateral face, lower back, lower extremity, nail, neck, periorbital region, posterior torso, scalp, and upper extremity (Table *4-2*). The medical sign and symptoms (Table *4-3*) of the five skin diseases were also included. A total of 41 features from patient information were extracted and used to develop the model.

Table 4-1: Number of images collected from Jimma and Dessie

Skin Condition	Number of images
Healthy	847
Acne Vulgaris	307
Atopic Dermatitis	300
Lichen Planus	289
Onychomycosis	211
Tinea capitis	269
Unknown	204
Total	**2427**

Table 4-2: Number of clinical images present in each anatomical site

Anatomical sites	Number of clinical images collected on each site				
	Acne vulgaris	Atopic dermatitis	Lichen planus	Onychomycosis	Tinea capitis
Upper extremity	-	107	77	-	-
Lower extremity	-	63	99	-	-
Periorbital	-	6	2	-	-
Armpit	-	11	7	-	-
Navel	-	2	-	-	-
Lower back	-	4	9	-	-
Scalp	-	-	1	-	269
Nail	-	-	-	211	-
Abdomen	-	-	4	-	-
Nose	-	-	3	-	-
Ear	-	-	1	-	-
Lateral face	183	45	26	-	-
Forehead	61	4	13	-	-
Anterior torso	23	23	26	-	-
Posterior torso	31	11	4	-	-
Chin	5	-	-	-	-
Neck	4	24	17	-	-
Total	**307**	**300**	**289**	**211**	**269**

Table 4-3: Medical signs and symptoms of five skin diseases

Diseases	Acne vulgaris	Atopic dermatitis	Lichen planus	Onychomycosis	Tinea capitis
Symptoms	• Blackheads • Whiteheads • Papules • Pimples • Nodule • cysts	• Dry skin • Scale • Bumps • Thickened cracked skin • Round patches of scaly skin	• Thickened nail • Purplish flat bumps • Lacy white on mouth lips or tongue • Painful sores in the mouth or vagina	• Nail discoloration • Nail shape distortion • Nail smell foul • Brittle crumby nail	• Scaly gray or reddened areas • Patches with black dots
Anatomical sites	• Lateral face • Forehead • Posterior torso • Anterior torso • Chin • Neck	• Neck • Lower extremity • Upper extremity • Anterior torso • Posterior torso • Lower back • Periorbital • Armpit • Lateral face • Forehead • Navel	• Lower extremity • Upper extremity • Lower back • Neck • Abdomen • Anterior torso • Lateral face • Nose • Ear • Scalp • Armpit • forehead	• Nail	• Scalp

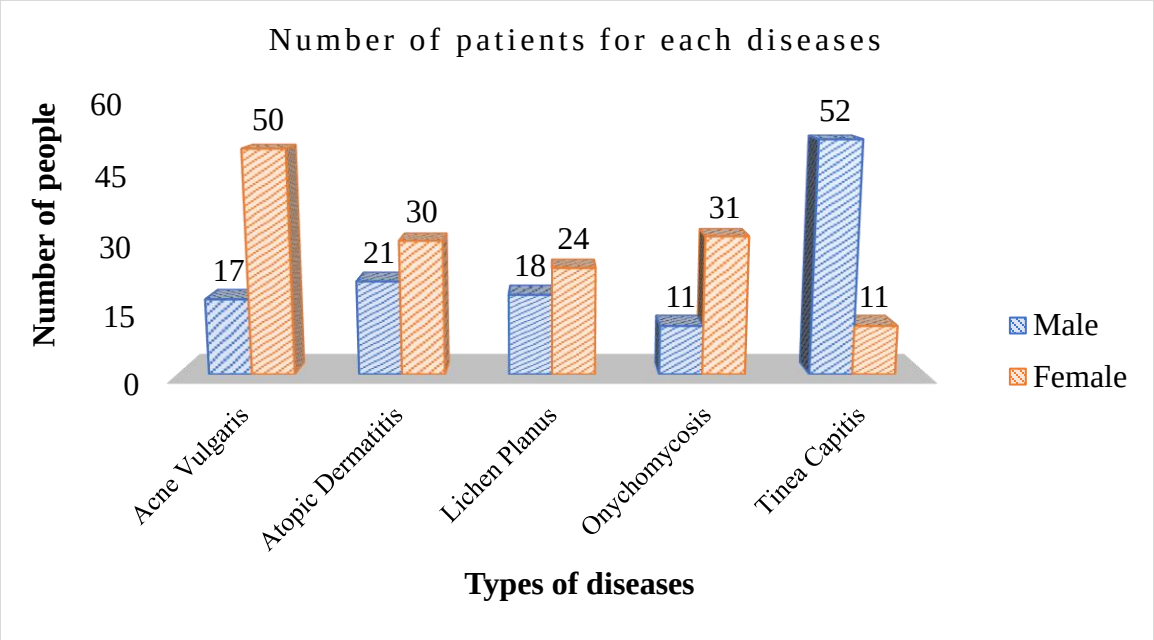

Figure 4.3: Number of patients of five skin conditions

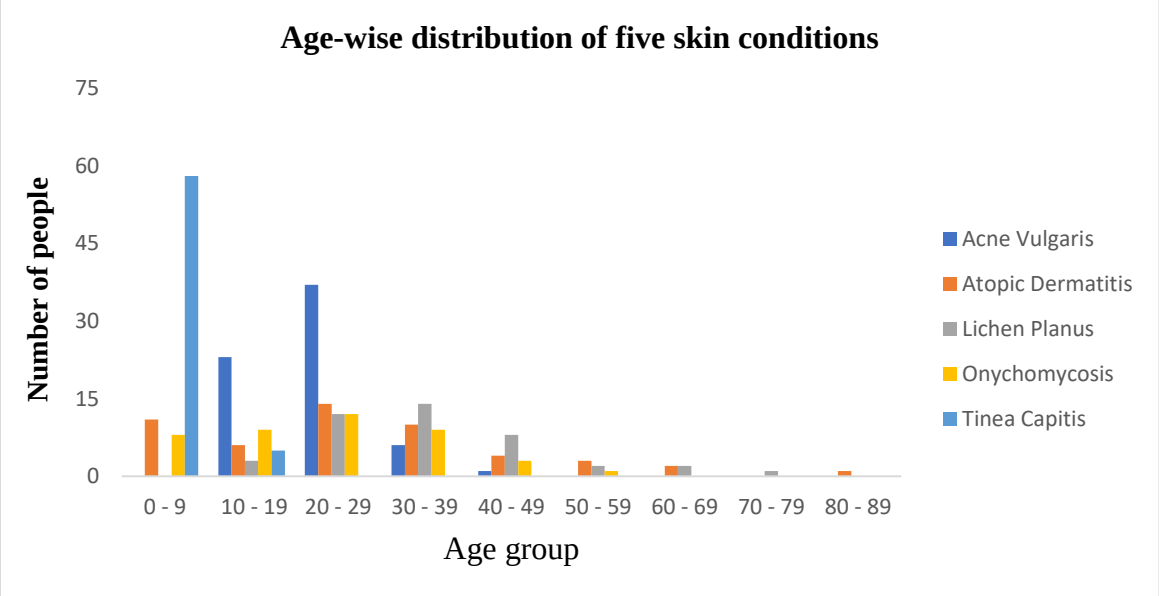

Figure 4.4: Age-wise distribution of five skin conditions

4.4.2. Data Preprocessing

Image resizing, color constancy, and data augmentation were applied to the collected images as a preprocessing step before model training. All the images were resized to 224 x 224 pixels to match the default input size of mobilent-v2 model that achieved the best accuracy. The dataset was split into 80 % for training (1264 images), 10% validation (158 images) and, 10% testing (158 images) before model training. The splitting was performed randomly while keeping the proportion of each disease (stratified). Then data augmentation was applied to the training dataset by 90° rotation, horizontal and vertical image flipping to increase the number of datasets. The patient information was converted to a feature vector using the one-hot encoding technique. Figure 4.5 shows the result of data augmentation.

Figure 4.5: Image resizing and data augmentation

4.4.2.1. Color constancy

The color of an object ‘s image depends on the incident light and object surface property. The human eye has the capability of perceiving constant color on the varying light condition, known as color constancy. Color constancy is a technique applied to compensate for the color bias resulting from varying illumination sources [54].

Computational color constancy mainly has two procedures. First estimating the illuminant and then reduce the color bias. The color of the illuminant was estimated using statistical and physics-based approaches. This study focused on the simplest and fast statistical-based color constancy technique, which includes the gray word [55], Max-RGB [56], and shades of gray [57] based on different assumptions. The gray world color constancy algorithm is mainly based on the assumption that the average surface reflectance of a typical scene is achromatic, i.e., gray. It

estimates the color of the illuminant as the average color of all pixels in the image using equation 4.1. Max-RGB estimates the color of the illuminant from the maximum response of the three-color channels (R-G-B). It assumes that a light incident on a white patch is unchanged after reflection that resulting in maximum camera response. Finally, the shades of gray algorithm extend the gray world for higher-order by using Makowski norm instead of averaging. The shades of gray approaches assume that the average of pixels raised to the power of **p** is gray as shown in Equation 4.2 below.

$$Ke_c = \frac{\int I_c(x)dx}{dx} \tag{4.1}$$

$$Ke_c = \left(\frac{\int I_c^p(x)dx}{\int dx}\right)^{\frac{1}{p}} \tag{4.2}$$

In the equations, P – is Makowski's norm and the shades of gray optimal illuminant estimate achieved at 6, e_c – the estimated color of the light, I_c– the RGB value of the pixel, K – normalization constant between 0 for no reflectance (black) and 1 for total reflectance (white) of the incident light, and X = (x, y) the position of the pixels. When P = 1, equation 4.2 is equal to the gray world assumption, when $p \rightarrow \infty$ equation 4.2 is equal to Max-RGB, and shade of gray is for $1 < P < \infty$.

The color of the light source was estimated using Equation 4.1 and 4.2 and the image was transformed using von Kries diagonal model [58].

$$\begin{pmatrix} I_R^t \\ I_G^t \\ I_B^t \end{pmatrix} = \begin{pmatrix} c_R & 0 & 0 \\ 0 & c_G & 0 \\ 0 & 0 & c_B \end{pmatrix} \begin{pmatrix} I_R \\ I_G \\ I_B \end{pmatrix} \tag{4.3}$$

Where [I_R, I_G, I_B] denotes the pixel values of the image under an unknown light source, [I^t_R, I^t_G, I^t_B] denotes the transformed pixel values and the matrix {c_R, c_G, c_B} are the scaling coefficient for color channels that relates the illuminant with the estimated color of the light e_c.

The shade of gray color constancy algorithm was used as a preprocessing step to remove the color bias of the clinical images. This algorithm was found to improve the classification accuracy of multisource images in literature [57]. The general procedure of the application of the shades of gray color constancy algorithm is depicted in Figure 4.6. Finally, the processed image was clipped

to [0, 255] to remove strange intensity values. The result of the shades of gray algorithm is shown in Figure *4.7*.

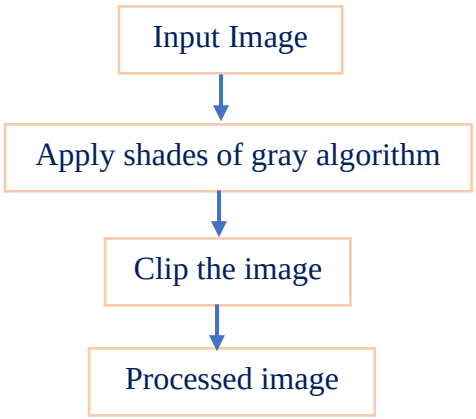

Figure 4.6: Block diagram of shades of gray algorithm implementation on images

Original image Shades of gray applied image

Figure 4.7: Shades of gray preprocessing result

4.4.2.2. One hot encoding

Converting a categorical variable into one-hot encoded vector enables a machine-learning algorithm to learn and predict well. The string values of gender, medical sign and symptoms, and anatomical site were one hot encoded to produce 40 features. Table *4-4* and Table *4-5* demonstrates a sample of one-hot encoding.

Table 4-4: One hot encoding (Anatomical sites)

Anatomical sites	Labels after encoding																
Abdomen	1	0	0	0	0	0	0	0	0	0	0	0	0	0	0	0	0
Anterior torso	0	1	0	0	0	0	0	0	0	0	0	0	0	0	0	0	0
Armpit	0	0	1	0	0	0	0	0	0	0	0	0	0	0	0	0	0
Chin	0	0	0	1	0	0	0	0	0	0	0	0	0	0	0	0	0
Ear	0	0	0	0	1	0	0	0	0	0	0	0	0	0	0	0	0
Forehead	0	0	0	0	0	1	0	0	0	0	0	0	0	0	0	0	0
Lateral face	0	0	0	0	0	0	1	0	0	0	0	0	0	0	0	0	0
Lower back	0	0	0	0	0	0	0	1	0	0	0	0	0	0	0	0	0
Lower Extremity	0	0	0	0	0	0	0	0	1	0	0	0	0	0	0	0	0
Nail	0	0	0	0	0	0	0	0	0	1	0	0	0	0	0	0	0
Navel	0	0	0	0	0	0	0	0	0	0	1	0	0	0	0	0	0
Neck	0	0	0	0	0	0	0	0	0	0	0	1	0	0	0	0	0
Nose	0	0	0	0	0	0	0	0	0	0	0	0	1	0	0	0	0
Periorbital	0	0	0	0	0	0	0	0	0	0	0	0	0	1	0	0	0
Posterior torso	0	0	0	0	0	0	0	0	0	0	0	0	0	0	1	0	0
Scalp	0	0	0	0	0	0	0	0	0	0	0	0	0	0	0	1	0
Upper extremity	0	0	0	0	0	0	0	0	0	0	0	0	0	0	0	0	1

Table 4-5: One hot encoding (Gender)

Gender	One hot encoding
Female	[1, 0]
Male	[0,1]

4.4.2.3. Label encoding

Label encoder converts a label from categorical to a number and the values were converted to code in alphabetic order. The labels categories are the name of the six skin conditions. The name of each label is replaced by a numerical value ("acne vulgaris" = 1). The age features were kept as it

is and the missing values of the unknown class were kept to zero. Table 4-6 indicates the label encoding result of the six skin conditions.

Table 4-6: Label encoding

Class labels	Labels after encoding
Acne Vulgaris	0
Atopic Dermatitis	1
Lichen Planus	2
Onychomycosis	3
Tinea capitis	4
Unknown	5

4.4.3. MobileNet-V2

MobileNet-v2 was introduced by Sandler et.al in 2019 [59], as a performance improvement of mobile models. It is based on an inverted residual structure where the input and output of the residual block are thin bottleneck layers opposite to traditional residual models. The architecture initially contains a fully convolutional layer with 32 filters followed by 19 residual bottlenecks. The fully convolution operation is replaced by depth-wise separable convolution that splits into two separable layers. First, depth-wise convolution performs light-weight filtering using 3 x 3 kernels per input channel. Following the depth-wise convolution, the point-wise convolution builds feature by computing a linear combination of the input images. The model parameters are smaller compared to other pre-trained models even from MobileNet model that makes it suitable for mobile and resource-limited environments. Figure 4.8 shows the architecture of MobileNet-V2 network.

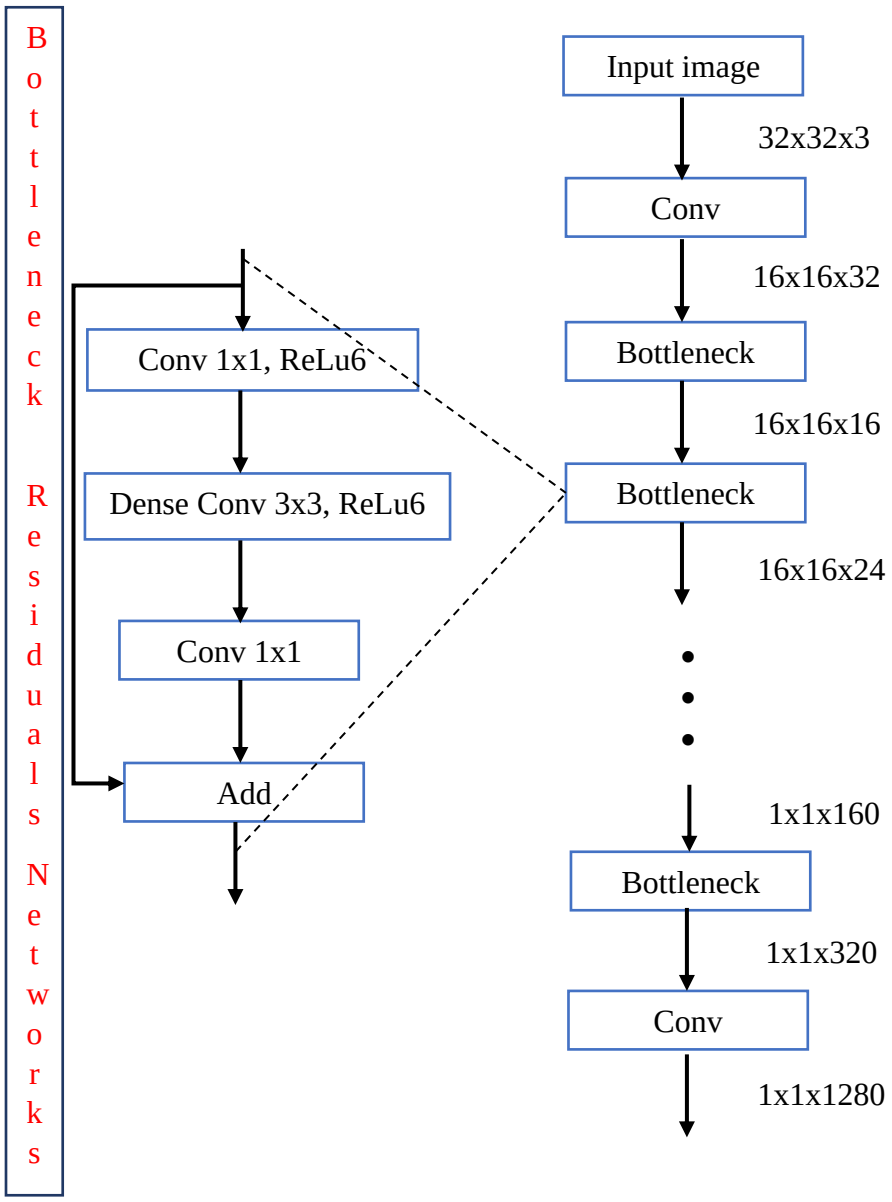

Figure 4.8: Architecture of Mobilenet-v2 model

There are different ways of repurposing the pre-trained model; fine-tuning, and using it as a fixed feature extractor. Fine-tuning the model is a technique for training some layers of the model while keeping other layers frozen. A pre-trained model can also be used as a fixed feature extractor by freezing the convolutional layers of the model. The extracted features are then fed to the classifier. It is suitable for resource-limited computation and small dataset size. In this study, mobilnet-v2 model was used as a fixed features extractor for multiclass classification using clinical images and patient information by freezing its convolutional base (freeze the whole architecture) and achieved the best result. Mobilnet-v2 model was fine-tuned for binary classification using clinical images. Freezing the convolutional base and setting the top layer to trainable achieved the best result for the multiclass classification problem. On the other hand, unfreezing the whole architecture of MobilNet_v2 model achieved the highest accuracy compared to freezing the convolutional base. The output features extracted by pre-trained mobilenet-v2 model is 1280. The result of the concatenation of all MobileNet_v2 model output with patient information is less than the result after feature reduction. Through trial and error, the best performance was achieved by reducing the image's feature to 128. Therefore, a dense layer with 128 neurons was added at the top of a pre-trained model for multiclass classification using images and patient information. On the other hand, all 1280 image features are directly fed to the classifier for binary and multiclass classification using images only. Sigmoid and SoftMax classifiers were used as binary and multiclass classifiers respectively. The SoftMax classifier interprets the scores as probabilities for each class and then encourages the probability of the correct class to be high which allows it to interpret its confidence in each class. Currently, the SoftMax classifier is used by many deep learning researchers. Only a dense layer and classifier are set to trainable. Figure *4.9* shows the overall methodology of the binary and multiclass classifier.

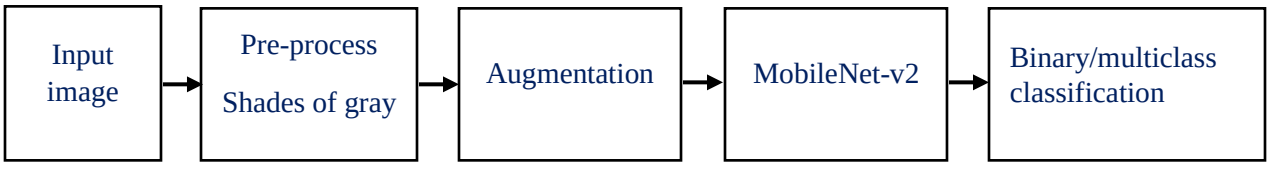

Figure 4.9: Overall methodology of the binary and multiclass classifier

The optimal model was developed by choosing the learning rate, optimizer, loss function, and batch size. Adam optimizer was chosen for this study because it converges faster and gives the

best accuracy [60]. The loss function used for binary and multiclass classification tasks is cross-entropy loss. The best result was found by setting the learning rate to 0.0001 for binary and multiclass classification Moreover, a weighted loss function based on labels frequency, which assigns more weight to less represented class, was applied to mitigate class imbalance in the dataset. The individual weight of a given class was computed using Equation 4.4

$$W_i = \frac{N}{n_i} \qquad (4.4)$$

where, W_i – indicates the weight of a given label i, N – the total number of the dataset, n_i – the number of samples of label i.

4.4.4. Feature concatenation

In this study, both the clinical image data and patient information were concatenated to classify the five common skin diseases. The patient information includes age (1), gender (2), anatomical site (17), and symptoms (21). Anatomical sites and symptoms of the diseases are depicted in Table *4-3*. The image features outputted from the pre-trained mobilenet-v2 model (1280) are larger than the patient information features (41). The image features are reduced to increase the influence of patient information and improve classification accuracy. To do so, a dense layer with neurons less than 1280 was added at the top of a pre-trained model and compared. The best result was found by adding 128 neurons. This reduces the output image features of the model to 128 and balances the two inputs types of the classifier (a one-hot encoded patient information features and the image features). The main reason behind using a neural network as a features reducer block is the added layer can be optimized along with the feature extractor and the classifier by including it in the backpropagation [61] computation. There are other approaches such as PCA [62], however, it is linear and the proposed approach is faster and simpler. Figure 4.10 summarizes a multiclass classifier using the image and patient information. The procedure includes first the image input fed to the pre-trained MobileNet_v2 model that is used as a features extractor. The output of the pre-trained model was fed to the neural network reducer block and outputted 128 image features. The extracted image features were concatenated with preprocessed patient information feature vectors. Feature concatenation is a technique used to join two or more arrays. Let A1 and A2 two arrays, concatenating along axis equal to 0 and 1 gives the result shown below.

A1 = [[1, 2], [3, 4]]

A2 = [[5, 6], [7,8]]

Concatenate = concatenate ((A1, A2), axis = 1) = [[1, 2, 5, 6], [3, 4, 7, 8]]

Concatenate = concatenate ((A1, A2), axis = 0) = [[1, 2], [3, 4], [5, 6], [7, 8]]

The clinical image was fed to a pre-trained mobilenet-v2 model. The model extracts meaningful and discriminating features and the extracted features were converted to one-dimensional array that can be used as an input for the next layer. On the other hand, forty-one hot encoded patient information features including anatomical site, diseases symptom, age, and gender information are available as an axillary input. The clinical image features and the auxiliary patient information features were concatenated and fed to the classifier as an input. Generally, the concatenation of 128 images feature and 41 patient information resulted in a total of 169 features. Later the concatenated features are fed to the classifier and the classifier returns the probability of the six classes. Figure *4.10* summarizes a multiclass classifier using clinical images and patient information.

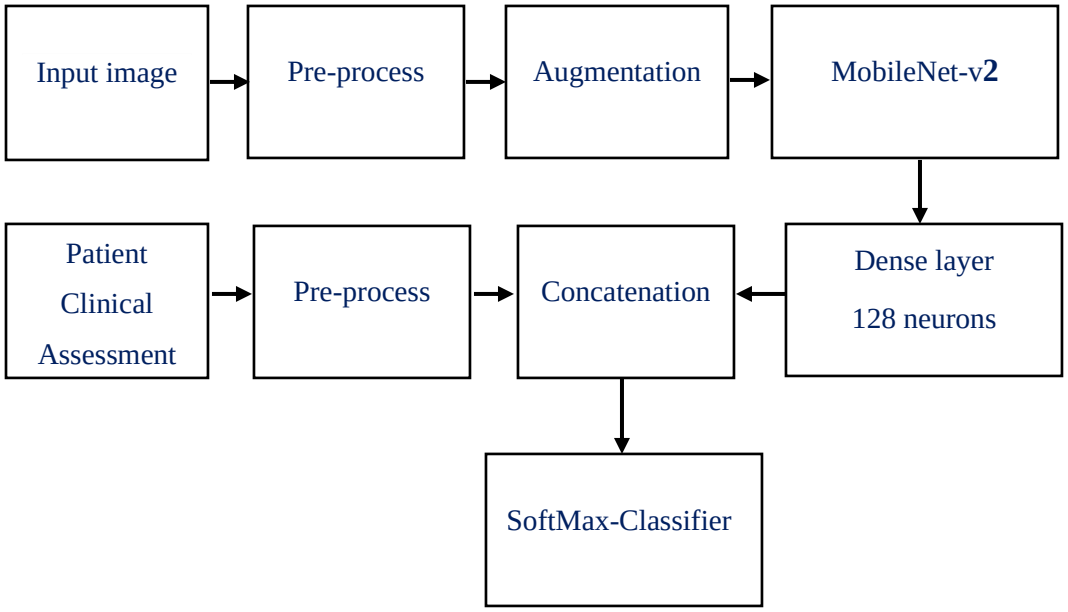

Figure 4.10: Block diagram of a multiclass classifier using clinical images and patient information

4.5. Performance Evaluation Metrics

The performance of the model was evaluated after model training. Accuracy, precision, recall, F1-score, and kappa score were used to evaluate the model performance. Confusion matrix (CM) is an M x M matrix that helps to measure the performance of the classification problem of two or more classes, where M is the number of target classes. It is useful for measuring accuracy, precision, recall, and F1- score. Accuracy measures the proportion of correct classification, precision measures the proportion of correct positive classification from positive prediction, and recall measures the proportion of correct positive prediction from the actual true. Moreover, specificity gives the proportion of negative prediction from the correct negative. The precision determines what proportion of positive prediction was correct. The receiver operator characteristic (ROC) curve is a graph that gives information about how the model correctly classifies positive and negative samples. The kappa value is a metric used to compare an observed accuracy with an expected accuracy or random chance. The performance evaluation metrics can be calculated using Equations 4.5 to 4.9. Table *4-7* shows the confusion matrix that enables to computation of different metrics.

Table 4-7: Confusion matrix

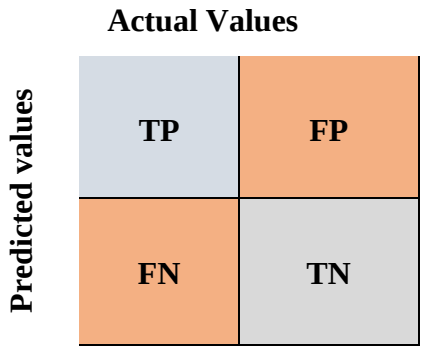

- True Positive (TP) value indicates the predicted abnormal skin condition matches the actual abnormal skin.
- True Negative (TN) value indicates that the predicted healthy skin condition is truly healthy.
- False Positive (FP) value indicates incorrect abnormal prediction while the actual class is healthy.

- False Negative (FN) value indicates incorrect healthy prediction while the actual class is abnormal.

$$precision = \frac{TP}{TP + FP} \tag{4.5}$$

$$Recall = \frac{TP}{TP + FN} \tag{4.6}$$

$$Accuracy = \frac{TP + TN}{TP + TN + FP + FN} \tag{4.7}$$

$$Specificity = \frac{TN}{TN + FP} \tag{4.8}$$

$$Kappa = \frac{observed\ accuracy - expected\ accuracy}{1 - expected\ accuracy} \tag{4.9}$$

4.6. Android App

A user-friendly android app was developed for the proposed automatic skin diseases diagnosis system using android studio. The script was written using Java programming language. The trained Pytorch model was converted to a torch script to run on mobile devices. Figure *4.11* shows the developed android application. The developed android application enables to diagnosis of five skin diseases by installing it on an Android-based smartphone. The user can select an image from the gallery or capture a new image by hitting the select and capture buttons respectively. “Site”, “Symptom “and “Gender” button enables the user to select the anatomical site, symptoms of the diseases, and gender respectively. The text box “Enter age” enables the user to provide their age. After all the required inputs are ready, the users can diagnose their skin condition by hitting the “Detect” button.

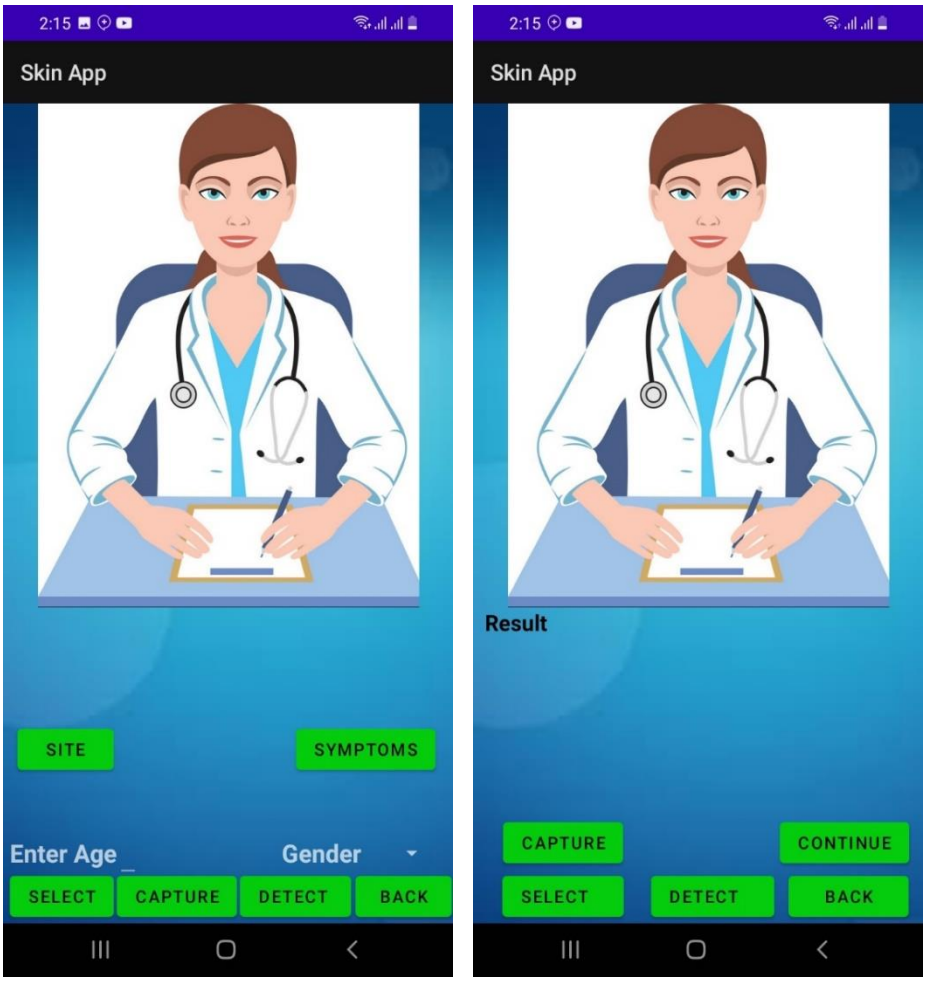

Figure 4.11: Developed android application

4.7. The material used in this research

The materials used in this study are listed below in Table 4-8.

Table 4-8: Material used for the proposed work

<table>
<tr><td>Software Materials</td><td colspan="3">Hardware materials</td></tr>
<tr><td rowspan="6">Python 3.7.6 software</td><td>Smartphone</td><td>Model</td><td>Camera</td></tr>
<tr><td>Nokia Window phone</td><td>Nokia 909</td><td>41Mp</td></tr>
<tr><td>Samsung Galaxy</td><td>Galaxy J6</td><td>13MP</td></tr>
<tr><td>Techno Spark4</td><td>KC8</td><td>13MP</td></tr>
<tr><td>SamsungA20</td><td></td><td>13MP</td></tr>
<tr><td rowspan="3">Android Studio 3.6.2

Matlab 2019</td><td colspan="3" rowspan="2">HP Pavilion Laptop 15-cs0xxx Intel(R) core (TM) i5-8250U CPU @1.6 GHz, 1.8 GHz, 4 core(s), 8 Logical Processor, 8GB RAM, 64bit operating system, x64 based processor, windows 10</td></tr>
</table>

Chapter 5

Results and discussions

5.1. Binary classification result

The total number of images used for training, validation, and testing was 1781, 221, and 221 respectively. The pre-trained mobilente-v2 model was trained for 25 epochs and 100% training, and 100% validation accuracy was achieved with the lowest validation loss of 0.003. Adam optimizer with a learning rate of 0.0001 was used to achieve this best accuracy. Figure 5.1 shows the training and validation accuracy curve, and training and validation loss curve of the binary classifier. The model correctly predicts all 221 unseen test images. The accuracy, precision, recall, F1 score, and kappa values of 100%, 100%, 100%, 1.00, and 100%, respectively were achieved on an unseen test dataset.

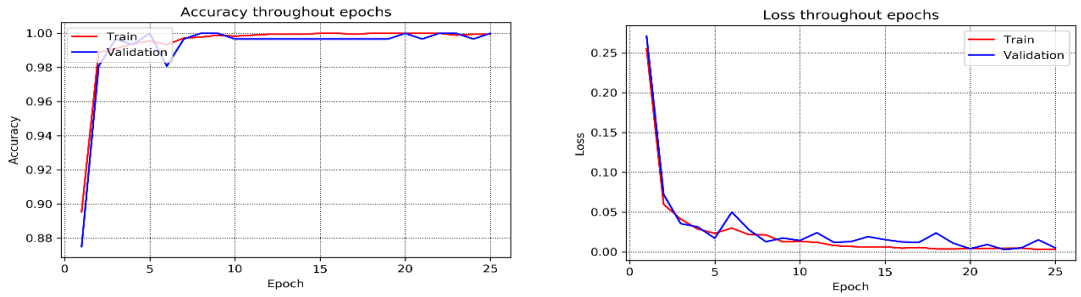

Figure 5.1: Summary of a binary classifier (left) training and validation accuracy (right) training and validation loss.

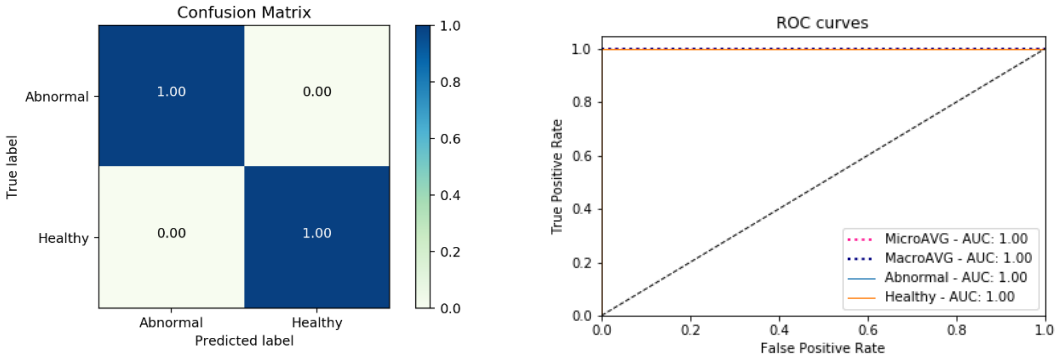

Figure 5.2: Normalized confusion matrix and ROC curve of the binary classification result. (Left) confusion matrix (Right) ROC curve

Figure 5.2 shows the experimental result of the binary classification in terms of confusion matrix and ROC curve. In addition, below in table 5-1 detail model, effectiveness scores are presented using accuracy, recall, precision, F1-score, and Kappa value.

Table 5-1: Precision and Recall report of a binary classifier on an independent test set

Skin Condition	Batch size	Learning rate	Precision (%)	recall (%)	f1-score (%)	Kappa score	Accuracy (%)
Abnormal	64	0.0001	100	100	100	1.00	100
Healthy			100	100	100		
		Average	100	100	100		

5.2. Multiclass classification

The total number of images used for training, validation, and testing was 1264, 158, and 158 respectively. A pre-trained mobilenet-v2 model was trained for 50 epochs using clinical images only. 94.2 % training and 88.3 % validation accuracy were achieved at the 45th epoch with the lowest validation loss of 0.306. The model has saved the best weight values at the 45th epoch for a final classification task. Figure *5.3* shows the accuracy and loss curve of the multiclass classifier. The model correctly classified 138 out of 158unseen test images. The model accuracy and loss on unseen test images were 87.9 and 0.333 respectively.

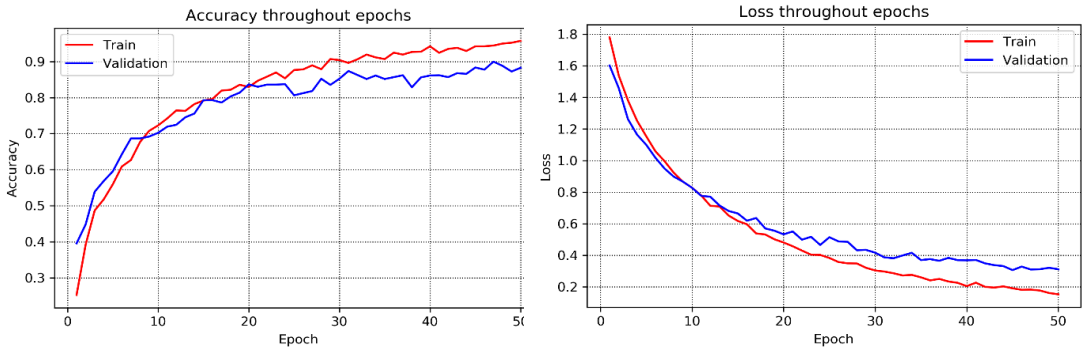

(a) (b)

Figure 5.3: Summary of a multi-class classifier using image only (a)training and validation accuracy (b)training and validation loss

Here below in Figure *5.4*, we present experimental results in terms of the confusion matrix and ROC curve. Moreover, in Table 5-2 summaries of details of multiclass classification results are presented.

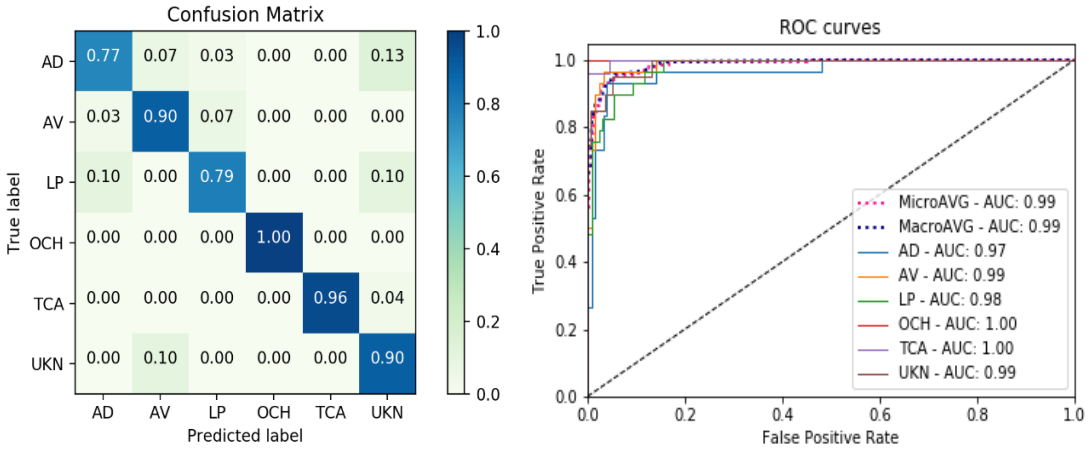

(a) (b)

Figure 5.4: Normalized confusion matrix and ROC curve of the multi-class classification using image only. (a) confusion matrix (b) ROC curve

Table 5-2: Precision recall repots of multiclass class classifier on unseen test dataset

Skin Condition	Precision (%)	recall (%)	f1-score (%)	Kappa score	Accuracy (%)
Acne Vulgaris	87	90	89	0.86	87.9
Atopic Dermatitis	85	77	81		
Lichen Planus	88	79	84		
Onychomycosis	100	100	100		
Tinea capitis	100	96	98		
Unknown	69	90	78		
Average	***88.2***	***88.7***	***88.3***		

5.3. Feature concatenation

The total number of images used for training, validation, and testing was 1264, 158, and 158 respectively along with the corresponding patient information. The pre-trained mobilente-v2 model was trained on using clinical images and patient information for 224 epochs. The model achieved 99.5% training and 97.9% validation accuracy at the 214th epoch with the lowest validation loss of 0. 084. The model correctly classified 153 images out of 157 test images. The model accuracy and loss on unseen test images were 97.5 and 0.074 respectively. Figure 5.5, and Table 5-3 summarize the detail of the multiclass classifier on images and patient information.

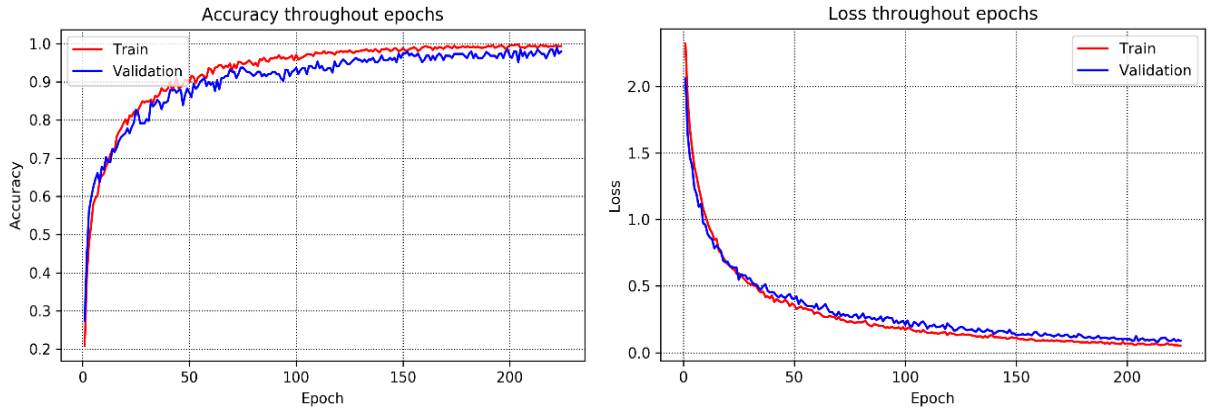

(a) (b)

Figure 5.5: Summary of a multi-class classifier using the image and patient information. (a)training and validation accuracy (b)training and validation loss

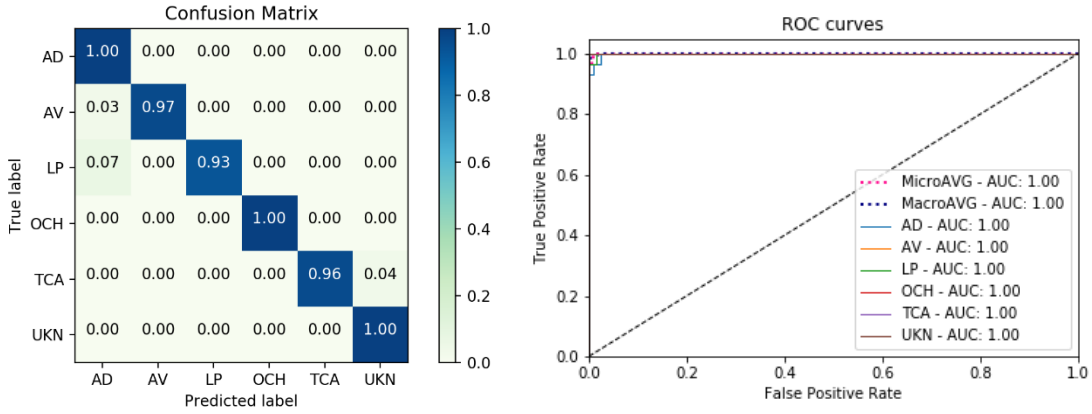

(a) (b)

Figure 5.6: The classification result on combination of image and patient information. (a) confusion matrix (b) ROC curve

Table 5-3: The classification metrics of the model on aggregated features

Skin Condition	Precision (%)	recall (%)	f1-score (%)	Kappa score	Accuracy (%)
Acne Vulgaris	91	100	95	**0.976**	**97.5**
Atopic Dermatitis	100	97	98		
Lichen Planus	100	93	96		
Onychomycosis	100	100	100		
Tinea capitis	100	96	98		
Unknown	95	100	98		
Average	***97.7***	***97.7***	***97.5***		

5.4. Android App

The developed android app is user-friendly and responds to the result within a fraction of a second. The first version of the application was distributed to end-users (expert dermatologist, general practitioners, MSc. Candidates, and residents from Addis Ababa and Jimma) for user acceptance testing and several feedbacks was accepted. They requested to present it in common local languages, a way to select multiple sites and symptoms, to modify the layout, and to include more skin diseases. Based on their request we updated the first version of the application and presented it as shown in Figure *5.7*. The sample format and result of user acceptance testing is shown in Table *5-4*. The first window of the app is designed for binary classification of the skin condition as Healthy or abnormal. The "Select" button enables to load of the clinical image from the device memory and the "Capture" button helps to capture a new image using the device camera. If the result of a binary classifier is abnormal the user can proceed by pressing the "Continue" button that pops up a new window for multiclass classification of the skin diseases into five categories. The "Detect" button enables to diagnosis of the skin condition fed to the model. The general procedure of diagnosing a skin disease using the developed android app is shown in Figure 5.7.

1. Open the App

2. Press select/ Capture button

3. Loaded image

4. Press detect Button

5. Press Continue

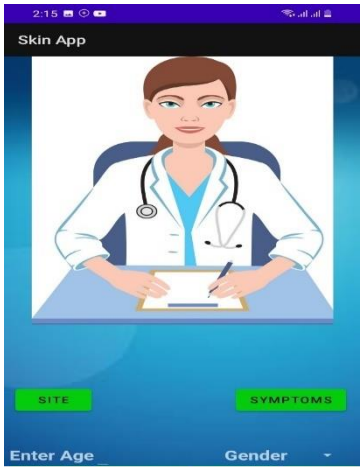

6. Load required info

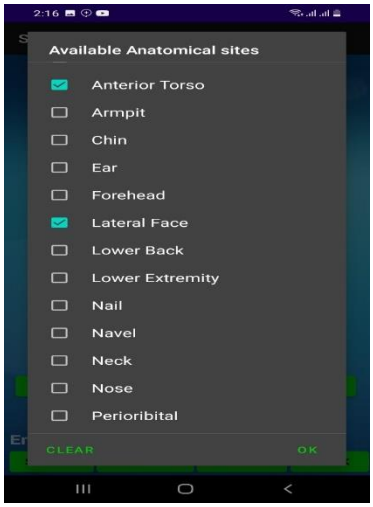

7. Detect

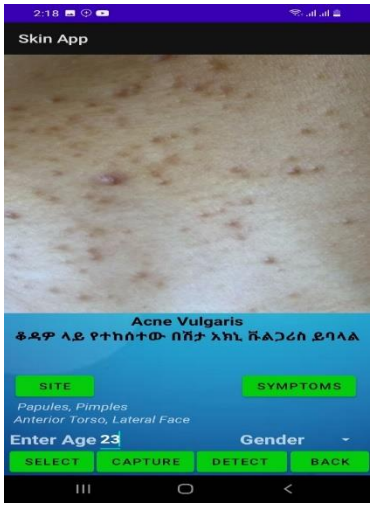

8. Back/Exit

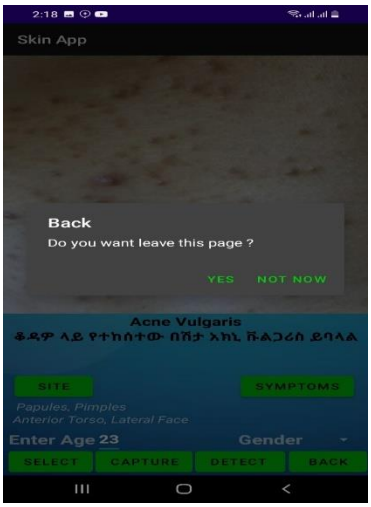

Figure 5.7: Procedure of diagnosing skin diseases using smartphone App

Table 5-4: sample queries for user acceptance testing

Questions	The number of people who participated	
	Accept	Reject
1. Application easiness to learn and use	20	0
2. Application compatibility to android versions	20	0
3. Time spends to diagnose (speed)	20	0
4. Memory and RAM requirement	20	0
5. Layout	20	0
6. Result of Acceptance	**Accepted**	

We get feedback from expert dermatologists and non-expert end-users on issues that are not included in this work. They asked us to include more diseases categories, incorporate additional patient information (anatomical sites and symptoms of the diseases), and include hints for medical terms (anatomical site, symptoms, and diseases name). We accept those issues as our limitations and will be solved near the future or other researchers can extend the work.

5.5. Discussion

Skin diseases are any condition that affects human skin. According to the global burden of diseases project, skin diseases are the fourth leading cause of non-fatal disease burden [3] which can affect almost 900 million people worldwide [2]. Skin diseases injure physical health and cause serious psychological problem: depression, frustration, and even suicidal ideation [26].

Skin diseases are commonly diagnosed using visual inspection, laboratory tests, imaging, and biopsy test. However, there are a limited number of sophisticated diagnostic devices and dermatologists, and even general practitioners, which hurdle the service delivery. Moreover, the common diagnostic techniques are tedious and require experience and excellent visual perception. Computer-aided diagnosis system has the potential to revolutionize the current diagnosis techniques enabling optimal treatment planning.

This study aimed to design and develop a smartphone-based automatic skin diseases diagnosis method using clinical images and patient information including age, gender, anatomical site of the diseases, and symptom list. A total of 1580 clinical images of six skin conditions were collected from the population of southwest Ethiopia (Dr. Gerbi Medium clinic, Jimma), Eastern Amhara, and the Afar region (Boru-Meda General Hospital), using different smartphone cameras with the corresponding patient data.

Table *4-2* demonstrated that anatomical sites were invaded by the five skin diseases. Tinea Capitis and Onychomycosis prefer scalp and nail respectively. On the other hand, Acne Vulgaris is more common in face and trunk regions. Atopic Dermatitis and Lichen Planus are more common on the upper and lower limbs and are also distributed around the trunk, neck, face, armpit. Medical signs and symptoms for the five skin diseases were used along with patient age, anatomical site, and gender.

A mobilenet-v2 model was trained using the collected data, first to identify normal skin from abnormal using images only and then uses a combination of skin images and patient information to identify the type of skin disease.

All images and patient information were pre-processed before model training. The color cast resulting from illumination variation was removed and the actual color of the images was restored by applying shades of gray color constancy algorithm [57]. After data pre-processing, the clinical

images along with the corresponding patient data were split to 80%, 10%, and 10% for training, validation, and testing, respectively. Data augmentation was applied by using the image transformation technique to increase the number of training data. The weighted loss function based on labels frequency was applied to tackle the class imbalance issue. A pre-trained Mobilent-v2 model was selected and fine-tuned for binary and multiclass classification for training since it is the best model for mobile devices and resource-limited environments.

For binary classification, the best result was achieved by applying a learning rate of 0.0001, a sigmoid activation function as a classifier, and cross-entropy loss as a loss function. The average accuracy, precision, recall, F1-score, and kappa score achieved were 100%, 100%, 100%, 100%, and 1.00 respectively. The multiclass classifier classifies the input clinical image into six different skin conditions. The unknown class was added as a sixth class to reduce the false-positive result. As a result, image lesions out of the five classes were classified as unknown. The best result was achieved by applying a learning rate of 0.00001, SoftMax activation function as a classifier, and weighted cross-entropy loss as a loss function. The model was tested using unseen datasets and evaluated using a variety of performance metrics. The average accuracy, precision, recall, F1-score, and kappa score were 87.9%, 88.2%, 88.7%, 89.8%, and 0.86, respectively, using images only (Table *5-2*). An improved performance was achieved using a combination of images and patient information. An average accuracy, precision, recall, F1-score, and kappa score of 97.5%, 97.7%, 97.7%, 97.5%, and 0.976, respectively were acquired after testing the model on the unseen dataset (Table *5-3*). Using the combined image and patient information increases the classification accuracy of the model by 9.6%.

Since there are about 3000 and more skin diseases [5], different researchers proposed machine learning and deep learning-based diagnosis systems for specific types of diseases [9–16]. Our study focused on the top 5 diseases that are common in Ethiopia. Even though the dataset used and the types of diseases considered were slightly different, the current work achieved significantly improved overall accuracy compared to [9–16] by incorporating patient information. A user-friendly android application also enables non-expert users to identify skin diseases using their smartphones. The developed system has the potential to be used as a decision support system for physicians, general practitioners, and patients. Table *5-5* shows the comparison between the proposed and previous studies.

Table 5-5: Comparison of the proposed study with previous works

Skin Condition	**Precision (%)**	**ROC**	**Accuracy (%)**
Nasr-Esfahani et al.	-		81
Fujisawa et al.	-		76.5
Hameed et al.	-		83
Han et al.	-	BCC = 0.96 SCC = 0.83 IEC = 0.82 MM = 0.96	-
Mendes et al.	-	-	78
Wu et al.	77	-	-
J. Velasco, et al.	-	-	94.4
Proposed work	***97.7***	***AD = 0.998*** ***AV = 1.0,*** ***LP = 0.999*** ***OCH = 1.0*** ***TCA = 1.0*** ***UKN = 1.0***	**97.5**

Chapter 6

Conclusion and Recommendation

6.1. Conclusion

The common procedures for diagnosing skin diseases are patient history and symptoms analysis, skin scraping, visual inspection, dermoscopic examination, and skin biopsy. However, those diagnosis methods are tedious, time-consuming, and prone to subjective diagnosis. There are sophisticated and robust medical imaging modalities available in the market. However, the cost of the equipment limits the affordability in a low-resource setting. Moreover, diagnostic techniques were proposed to diagnose skin cancer and tumors. However, the dataset used is mainly composed of a white-skinned population, concentrated on diagnosis on cancer and tumor and the accuracy reported the need to be improved.

The proposed study enables to automatic diagnosis of five common skin diseases using the clinical image and patient information. The color cast introduced due to various illumination sources were corrected using the shades of gray color constancy algorithm. Data augmentation techniques were applied to increase the training dataset before training the pre-trained mobilenet-v2 model. Patient information was encoded to a feature vector using one-hot encoding technique. Clinical image features were extracted using pre-trained mobilenet-v2 and the output feature vector was concatenated with one hot encoded patient information. The best classification accuracy achieved by the multiclass classifier using image only and combination of clinical images and patient information was 87.9% and 97.5% respectively. The model performance was improved by 9.6% on a combination of clinical images and patient information. Moreover, the proposed excels the previous high-performing works by 3.1%. Additionally, the pattern of skin diseases in southwest Ethiopia was investigated. Inflammatory skin conditions were prevalent compared to cancerous skin conditions. The developed diagnostic system assists dermatologists, general practitioners, health practitioners in rural areas, and for self-assessment of skin conditions.

Based on our plan, in this research, we tried to identify the prevalent skin condition in southwest Ethiopia and develop an automated android-based skin diseases diagnosis system. However, the dataset we collected was small for experimentation.

6.2. Recommendation

The proposed model was developed using small datasets collected from southwest Ethiopia and south Wollo. Even though the proposed work gave a good result, it is better to increase the dataset size by collecting more data from all regions of the country so that the model generalization capability will improve. Therefore, it is recommended to collect more datasets from different places.

Moreover, the study was limited to diagnosing only five skin diseases. Therefore, including more skin conditions, such as seborrheic dermatitis, scabies, lichen simplex chronicus, and Ecthymia contagiosum is very important for dermatological care.

Finally, we recommend developing an ensemble model, a model that can diagnose diseases using images, and a knowledge base system that diagnoses diseases using patient information or other input, which can further boost the performance.

References

[1] W. D. James, T. G. Berger, D. M. Elston, and R. B. Odom, "Andrews' diseases of the skin : clinical dermatology.," in *Andrews' diseases of the skin: clinical dermatology 1990*, 1990, pp. ix–1062.

[2] "Recognizing neglected skin diseases." World Health Organization Global, 2018.

[3] D. Seth, K. Cheldize, D. Brown, and E. F. Freeman, "Global burden of skin disease: inequities and innovations. Current dermatology reports," *PMC*, vol. 6(3), pp. 204–10, 2017.

[4] A. G. Kelbore, P. Owiti, A. J. Reid, E. A. Bogino, and L. Wondewosen, "Pattern of skin diseases in children attending a dermatology clinic in a referral hospital in Wolaita Sodo , southern Ethiopia," *BMC Dermatol.*, vol. 19(1), pp. 1–8, 2019.

[5] L. Tizek, M. . Schielein, F. Seifert, T. Biedermann, A. Bohner, and A. Zink, "Skin diseases are more common than we think: screening results of an unreferred population at the Munich Oktoberfest," *J. Eur. Acad. Dermatology Venereol.*, vol. 33(7), pp. 1421–8, 2019.

[6] S. Nutten, "Atopic Dermatitis : Global Epidemiology and Risk Factors," *Ann. Nutr. Metab.*, vol. 66(suppl.1, pp. 8–16, 2015.

[7] A. K. Gupta *et al.*, "Global perspectives for the management of onychomycosis," *Int. J. Dermatol.*, vol. 58(10), pp. 1118–29, 2019.

[8] T. B. Tufa and D. W. Denning, "The Burden of Fungal Infections in Ethiopia," *J. Fungi*, vol. 5(4), p. 109, 2019.

[9] A. P. Bonechi S, Bianchini M, Bongini P, Ciano G, Giacomini G, Rosai R, Tognetti L, Rossi A, "Fusion of Visual and Anamnestic Data for the Classification of Skin Lesions with with Deep Learning," in *International Conference on Image Analysis and Processing*, 2019, pp. 211–219.

[10] C. T. Chin YP, Hou ZY, Lee MY, Chu HM, Wang HH, Lin YT, Gittin A, Chien SC, Nguyen PA, Li LC, "A patient-oriented, general-practitioner-level, deep-learning-based cutaneous pigmented lesion risk classifier on a smartphone," *Br. J. Dermatol.*, vol. 182(6), pp. 1498–

1500, 2020.

[11] Y. Fujisawa *et al.*, "Deep learning-based, computer -aided classifier developed with a small dataset of clinical images surpasses board-certified dermatologists in skin tumor diagnosis," *Br. J. Dermatol.*, vol. 180(2), pp. 373–81, 2019.

[12] N. Hameed, A. Shabut, and M. A. Hossain, "A Computer-aided diagnosis system for classifying prominent skin lesions using machine learning," in *2018 10th Computer Science and Electronic Engineering (CEEC)*, 2018, pp. 186–191.

[13] S. S. Han, M. S. Kim, W. Lim, G. H. Park, and I. Park, "Classification of the Clinical Images for Benign and Malignant Cutaneous Tumors Using a Deep Learning Algorithm," *J. Invest. Dermatol.*, vol. 138(7), pp. 1529–38, 2018.

[14] D. B. Mendes and N. C. da Silva, "Skin Lesions Classification Using Convolutional Neural Networks in Clinical Images," *arXiv Prepr. arXiv1812.02316*, 2018.

[15] E. Nasr-Esfahani *et al.*, "Melanoma Detection by Analysis of Clinical Images Using Convolutional Neural Network," in *2016 38th Annual International Conference of the IEEE Engineering in Medicine and Biology Society (EMBC)*, 2016, pp. 1373–1376.

[16] F. Nunnari, C. Bhuvaneshwara, A. O. Ezema, and D. Sonntag, "A study on the fusion of pixels and patient metadata in CNN-based classification of skin lesion images.," in *International Cross-Domain Conference for Machine Learning and Knowledge Extraction*, 2020, pp. 191–208.

[17] A. G. C. Pacheco, A. Ali, and T. Trappenberg, "Skin cancer detection based on deep learning and entropy to detect outlier samples," *arXiv Prepr. arXiv1909.04525*, pp. 1–6, 2019.

[18] A. G. C. Pacheco and R. A. Krohling, "The impact of patient clinical information on automated skin cancer detection," *Comput. Biol. Med.*, vol. 116, p. 103545, 2020.

[19] J. Ruiz-castilla and J. Rangel-cortes, "CNN and Metadata for Classi fi cation of Benign and Malignant Melanomas," in *International Conference on Intelligent Computing*, 2019, pp. 569–579.

[20] K. Sriwong, S. Bunrit, K. Kerdprasop, and N. Kerdprasop, “Dermatological Classification Using Deep Learning of Skin Image and Patient Background Knowledge,” *Int. J. Mach. Learn. Comput.*, vol. 9, pp. 862–7, 2019.

[21] J. Velasco *et al.*, “A Smartphone-Based Skin Disease Classification Using MobileNet CNN,” *arXiv Prepr. arXiv1911.07929*, vol. 8(5), pp. 3–8, 2019.

[22] Z. H. E. Wu *et al.*, “Studies on Different CNN Algorithms for Face Skin Disease Classification Based on Clinical Images,” *IEEE Access*, vol. 7, pp. 66505–11, 2019.

[23] R. . Weller, J. A. A. Hunter, John A. Savin, and M. V. D. BA, *Clinical Dermatology*, Fourth Edi. Blackwell Publishing, 2014.

[24] M. Hoffman, “Picture of the Skin Human Anatomy,” *WebMD*. 2014.

[25] D. J. Birmingham, “Overview: occupational skin diseases,” *Encycl. Occup. Heal. Saf.*, vol. 4, pp. 12–1, 1998.

[26] A. Bewley, “The neglected psychological aspects of skin disease,” *BMJ*, vol. 3208, pp. 1–2, 2017.

[27] S. M. Tuchayi, E. Makrantonaki, R. Ganceviciene, C. Dessinioti, S. R. Feldman, and C. C. Zouboulis, “Acne vulgaris,” *Nat. Rev. Dis. Prim.*, vol. 1(1), pp. 1–20, 2015.

[28] K. Gebauer, “Acne in adolescents,” *Aust. Fam. Physician*, vol. 46(12), pp. 892–5, 2017.

[29] L. A. D. S. G.N, Villar, J.F.Filho, “Quality of life, self-esteem and psychosocial factors in adolescents with acne vulgaris,” *An. Bras. Dermatol.*, vol. 90, pp. 622–9., 2015.

[30] J. I. Silverberg, “Public health burden and Epidemiology of Atopic Dermatitis,” *Dermatol. Clin.*, vol. 35(3), pp. 283–289, 2017.

[31] F. Gorouhi, P. Davari, and N. Fazel, “Cutaneous and mucosal lichen planus: a comprehensive review of clinical subtypes, risk factors, diagnosis, and prognosis,” *Sci. World J.*, vol. 2014, 2014.

[32] H. A. Agel M, Al-Chihabi M, Zaitoun H, Thornhill MH, “Lichen Planus in Children,” *Dent. Update*, vol. 45(3), pp. 227–34, 2018.

[33] S. R. Lipner and R. K. Scher, “Onychomycosis Clinical overview and diagnosis,” *J. Am. Acad. Dermatol.*, vol. 80(4), pp. 835–51, 2019.

[34] G. M. Solís-Arias MP, “Onychomycosis in children . A review,” *Int. J. Dermatol.*, vol. 56(2), pp. 123–30, 2017.

[35] R. J. Hay, “Tinea Capitis : Current Status,” *Mycopathologia*, vol. 182(1), pp. 87–93, 2017.

[36] F. S. Gupta AK, Mays RR, Versteeg SG, Piraccini BM, Shear NH, Piguet V, Tosti A, “Tinea capitis in children: a systematic review of management,” *J. Eur. Acad. Dermatology Venereol.*, vol. 32(12), pp. 2264–74, 2018.

[37] B. Felix *et al.*, “Estimation of the Burden of Tinea Capitis Among Children in Africa,” *Mycoses*, vol. 64(4), pp. 349–63, 2021.

[38] S. L. Schneider, I. Kohli, I. H. Hamzavi, M. L. Council, A. M. Rossi, and D. M. Ozog, “Emerging imaging technologies in dermatology: Part I: Basic principles,” *J. Am. Dermatology*, vol. 80(4), pp. 1114–20, 2019.

[39] I. Hernandez-Neuta *et al.*, “Smartphone-based clinical diagnostics : towards democratization of evidence-based health care,” *J. Intern. Med.*, vol. 285(1), pp. 19–39, 2019.

[40] L. M. Abbott, R. S. Magnusson, E. Gibbs, and S. D. Smith, “Smartphone use in dermatology for clinical photography and consultation: current practice and the law,” *Australas. J. Dermatol.*, vol. 59(2), pp. 101–7, 2016.

[41] C. Boissin, J. Fleming, L. Wallis, M. Hasselberg, and L. Laflamme, “Can we trust the use of smartphone cameras in clinical practice? Laypeople assessment of their image quality,” *Telemed. e-HEALTH*, vol. 21(11), pp. 887–92, 2015.

[42] J. B. Wagner, “Artificial Intelligence in Medical Imaging,” *Radiol. Technol.*, vol. 90(5), pp. 489–501, 2019.

[43] T. Folke, S. C. Yang, S. Anderson, and P. Shafto, “Explainable AI for medical imaging: explaining pneumothorax diagnoses with Bayesian teaching,” *arXiv Prepr. arXiv2106.04684*, pp. 1–20, 2021.

[44] S. J. Lewis, Z. Gandomkar, and P. C. Brennan, “Artificial Intelligence in medical imaging practice : looking to the future,” *J. Med. Radiat. Sci.*, vol. 66(4), pp. 292–5, 2019.

[45] D. Jarrett, E. Stride, K. Vallis, and M. J. Gooding, “Applications and limitations of machine learning in radiation oncology,” *Br. J. Radiol.*, vol. 92(1100), pp. 1–12, 2019.

[46] D. T. Hogarty *et al.*, “Artificial Intelligence in Dermatology — Where We Are and the Way to the Future : A Review,” *Am. J. Clin. Dermatol.*, vol. 21(1), pp. 41–7, 2020.

[47] J. Latif, C. Xiao, A. Imran, and S. Tu, “Medical imaging using machine learning and deep learning algorithms: a review,” in *2019 2nd International Conference on Computing, Mathematics and Engineering Technologies (iCoMET)*, 2019, pp. 1–5.

[48] B. Reig, L. Heacock, K. J. Geras, and L. Moy, “Machine Learning in Breast MRI,” *J. Magn. Reson. Imaging*, vol. 52(4), pp. 998–1018, 2020.

[49] J.-G. AU - Lee *et al.*, “Deep Learning in Medical Imaging: General Overview,” *Korean J. Radiol.*, vol. 18(4), pp. 570–84, 2017.

[50] E. Klang, “Deep learning and medical imaging,” *J. Thorac. Dis.*, vol. 10(3), pp. 1325–1328, 2018.

[51] J. Wang, H. Zhu, S. Wang, and Y. Zhang, “A Review of Deep Learning on Medical Image Analysis,” *Mob. Networks Appl.*, vol. 5, pp. 1–30, 2020.

[52] B. Kieffer, M. Babaie, S. Kalra, and H. R. Tizhoosh, “Convolutional Neural Networks for Histopathology Image Classification : Training vs . Using Pre-Trained Networks,” in *2017 Seventh International Conference on Image Processing Theory, Tools and Applications (IPTA)*, 2017, pp. 1–6.

[53] M. Simon, E. Rodner, and J. Denzler, “ImageNet pre-trained models with batch normalization,” *arXiv Prepr. arXiv1612.01452.*, 2016.

[54] G. D. Finlayson, “Computational colour constancy,” in *Proceedings 15th International Conference on Pattern Recognition. ICPR-2000*, 2000, pp. 191–196.

[55] G. Buchsbaum, “A Spatial Processor Model for Object Colour Perception,” *J. Franklin Inst.*, vol. 310(1), pp. 1–26, 1980.

[56] E. H. Land and E. H. Land, “The Retinex Theory of Color Vision,” *Sci. Am.*, vol. 237(6), pp. 108–29, 1977.

[57] E. Finlayson, Graham, Trezzi, “Shades of Gray and Colour Constancy,” in *Color and Imaging Conference, 12th Color and Imaging Conference Final Program and Proceedings*, 2004, pp. 37–41.

[58] J. von Kries, “Influence of adaptation on the effects produced by luminous stimuli.” handbuch der Physiologie des Menschen, pp. 109–282, 1905.

[59] M. Sandler, M. Zhu, A. Zhmoginov, and C. V Mar, “MobileNetV2: Inverted Residuals and Linear Bottlenecks,” in *Proceedings of the IEEE conference on computer vision and pattern recognition*, 2018, pp. 4510–4520.

[60] D. R. Adrian, *Deep Learning for computer vision: practitioner Bundle)*, 1st Editio. PyImageSearch, 2017.

[61] W. R. Rumelhart DE, Hinton GE, “Learning representations by back-propagating errors,” *Nature*, vol. 323(6088), pp. 533–6, 1986.

[62] L. J. Williams, “Principal component analysis ′,” *Wiley Interdiscip. Rev. Comput. Stat.*, vol. 2(4), pp. 433–459, 2010.

Appendices

Appendix A: **Format for collecting Clinical Image and patient information**

Automated Skin diagnosis using deep learning form clinical images and patient clinical assessment

By: Kedir Ali

Tips during data collection

1. ***Age:*** *Float value and Range will be taken Later*
2. ***Sex:*** *Male or Female*
3. ***Ethnicity:*** *Black…*
4. ***Symptoms****: Bothersome in appearance, bleeding, increase in size, darkening, itching, burning, painful:*

   Response – Yes/NO/Unknown

5. ***Medical Sign:*** *Fever, chills, fatigue, joint pain, mouth, sore, shortness of breath: Yes/No/Unknown*
6. ***Duration of the skin problem persisted:***

   One day/ less than one week/ one week/ two weeks/ one -four week/ one month/ one -three month/ three month / three to six month/ six month/ one year/ more than one year/ more than five years/ since child hood/ since birth/ unknown
7. ***Frequency of occurrence:*** *Always present / comes and goes*
8. ***Personal History and Family History:*** *Yes/ No*
9. ***Anatomical site***

Sample format of data collection

ID	Age	Sex	Ethnicity	Symptoms	Medical Signs	Duration	frequency	Personal history	Family history	Location	Diagnosis
001											
002											
003											
004											
019											

Appendix B: Analysis result of the pattern of skin diseases in southwest Ethiopia

Table 0-1 Analysis result of the pattern of skin diseases in southwest Ethiopia

No.	Diseases	Total Number of patient (%)	Males (%)	Females (%)	Mean_Age
1	Atopic dermatitis	600 (7.21)	271 (55.65)	216 (44.35)	18.942
2	Rosacea	37 (0.44)	10 (30.3)	23 (69.7)	30.647
3	Acne Vulgaris	507 (6.09)	124 (29.8)	301 (70.82)	21.345
4	Lichen Planus	275 (3.3)	132 (51.56)	124(48.44)	33.661
5	Lichen Nitidus	4 (0.05)	1 (33.33)	2 (66.67)	21.667
6	Lichenoid Eruption	19 (0.23)	11 (78.57)	3 (21.43)	33.6
7	Vitiligo	435 (5.23)	211 (55.38)	170 (44.62)	26.401
8	Leishmaniasis	47 (0.56)	13 (40.63)	19 (59.38)	22.744
9	Pyoderma	220 (2.64)	117 (60.62)	76 (39.38)	18.727
10	Paronychia	82 (0.98)	18 (28.13)	46 (71.88)	26.838
11	Tinea Capitis	524 (6.29)	275 (62.08)	168 (37.92)	5.944
12	Onychomycosis	147 (1.77)	48 (40)	72 (60)	27.016
13	Scabies	525 (6.31)	294 (68.53)	135 (31.47)	16.862
14	Cellulitis	96 (1.15)	39 (49.37)	40 (50.63)	27.072
15	Cheilitis	61 (0.73)	37 (72.55)	14 (27.45)	30.667
16	Contact dermatitis	209 (2.51)	104 (55.03)	85 (44.97)	34.149
17	Seborrheic Dermatitis	423 (5.08)	199 (57.35)	148 (42.65)	25.533
18	Erythrasma	54 (0.65)	29 (69.05)	13 (30.95)	30.277
19	Acute Urticaria	164 (1.97)	69 (48.59)	73 (51.41)	30.447
20	Papular Urticaria	195 (2.34)	97 (54.8)	80 (45.2)	2.914
21	Chronic Urticaria	136 (1.63)	46 (43.81)	59 (56.19)	32.882
22	Pityriasis Alba	173 (2.08)	63 (46.67)	72 (53.33)	11.799
23	Bursitis	1 (0.01)			

24	Psoriasis	88 (1.06)	52 (66.67)	26 (33.33)	27.784
25	Candidal intertigo	86 (1.03)	23 (36.51)	40 (63.49)	23.671
26	Hemangioma	7 (0.08)	2 (33.33)	4 (66.67)	9.667
27	Molluscum Contagiosum	31 (0.37)	18 (62.07)	11 (37.93)	7.133
28	Corn	7 (0.08)	3 (75)	1 (25)	33.667
29	Vascular Ulcer	1 (0.01)			
30	Nummular Ezcema	33 (0.4)	13 (46.43)	15 (53.57)	24.25
31	Aphthous Ulcer	5 (0.06)	2 (100)		34.333
32	Atrophic Secondary burn	4 (0.05)		2 (100)	21
33	Abscess	17 (0.2)	6 (42.86)	8 (57.14)	21.25
34	Tinea Corporis	183 (2.2)	59 (45.04)	72 (54.96)	28.589
35	Tinea Manuum	55 (0.66)	16 (34.78)	30 (65.22)	27.708
36	Erythroderma	36 (0.43)	17 (60.71)	11 (39.29)	30.429
37	Lichen Simplex chronicus	422 (5.07)	213 (60.17)	141 (39.83)	26.504
38	Folliculitis	92 (1.11)	29 (38.67)	46 (61.33)	18.103
39	Tropical Ulcer	3 (0.04)	1 (100)		17
40	Tinea cruris	71 (0.85)	21 (72.41)	8 (27.59)	31.66
41	Candidiasis	60 (0.72)	23 (40.35)	34 (59.65)	10.053
42	Keloid	59 (0.71)	25 (51.02)	24 (48.98)	27.288
43	Prurigo	100 (1.2)	46 (55.42)	37 (44.58)	20.6
44	Melasma	161 (1.93)	38 (27.14)	102 (72.86)	28.458
45	Seborrheic Melasma	116 (1.39)	60 (63.16)	35 (36.84)	30.694
46	Impetigo	143 (1.72)	62 (50)	62 (50)	7.611
47	Periorificial dermatitis	9 (0.11)	1 (12.5)	7 (87.5)	23.625
48	Angioderma	19 (0.23)	11 (78.57)	3 (21.43)	23.533
49	Onchodermatitis	1 (0.01)			

50	Tinea Facciei	53 (0.64)	20 (47.62)	22 (52.38)	13.468
51	Tinea Incognito	55 (0.66)	16 (44.44)	20 (55.56)	28.364
52	Kerion	55 (0.66)	30 (65.22)	16 (34.78)	7.319
53	Epidermal Nevus	6 (0.07)		2 (100)	8.5
54	Pityriasis Versicolor	67 (0.8)	36 (54.55)	30 (45.45)	22.364
55	Chicken Pox	67 (0.8)	37 (58.73)	26 (41.27)	16.825
56	Alopecia Areata	76 (0.91)	46 (59.74)	31 (40.26)	23.408
57	Tinea Versicolor	25 (0.3)	11 (55)	9 (45)	29.409
58	Wart	77 (0.92)	41 (57.75)	30 (42.25)	27.069
59	Tinea Pedis	106 (1.27)	53 (53)	47 (47)	36.322
60	Marjolin Ulcer	2 (0.02)	1 (100)		63
61	Osteoma cutis	1 (0.01)			
62	Squamous cell carcinoma	21 (0.25)	9 (52.94)	8 (47.06)	49
63	Erosio interdigitalis	14 (0.17)	1 (9.09)	10 (90.91)	24.077
64	Soft tissue tumor	31 (0.37)	11 (50)	11 (50)	22.44
65	Keratoderma	31 (0.37)	10 (37.04)	17 (62.96)	26.536
66	Vulvovaginal Candidiasis	28 (0.34)		19 (100)	27.632
67	Follicular Ezcema	16 (0.19)	6 (66.67)	3 (33.33)	30.917
68	Sebopsoriassis	11 (0.13)	4 (44.44)	5 (55.56)	43.2
69	Leprosy	22 (0.26)	18 (90)	2 (10)	37
70	Secondary Harrison syndrome	1 (0.01)			
71	Xerosis	32 (0.38)	14 (58.33)	10 (41.67)	23.222
72	Podoconosis	18 (0.22)	6 (42.86)	8 (57.14)	43.75
73	Pruritus	13 (0.16)	10 (76.92)	3 (23.08)	36.769
74	Caterpillar Dermatitis	11 (0.13)	5 (55.56)	4 (44.44)	26.545
75	Pityriasis Rosea	25 (0.3)	3 (13.04)	20 (86.96)	20.64
76	Shoe Dermatitis	19 (0.23)	7 (41.18)	10 (58.82)	33.895

77	Tinea Interdigitale	9 (0.11)	5 (62.5)	3 (37.5)	24.111
78	Herpes Zoster	35 (0.42)	21 (61.76)	13 (38.24)	39
79	Epidermodysplasia verruciformis	2 (0.02)	2 (100)		25
80	Carbuncle	6 (0.07)	2 (33.33)	4 (66.67)	16.667
81	Furuncle	32 (0.38)	18 (56.25)	14 (43.75)	28.063
82	Melanocytic Naevus	5 (0.06)	1 (20)	4 (80)	19
83	Eczema	176 (2.11)	90 (54.88)	74 (45.12)	28.22
84	Dyschromia	1 (0.01)	1 (100)		17
85	Ecthymia Contagiosum	271 (3.26)	147 (53.26)	129 (46.74)	23.192
86	Morphia	6 (0.07)	3 (50)	3 (50)	28.833
87	Chromomycosis	1 (0.01)	1 (100)		31
88	Balanopestisis	1 (0.01)	1 (100)		17
89	Verruca Vulgaris	9 (0.11)	7 (77.78)	2 (22.22)	21
90	Discoid lupus erythematosus	22 (0.26)	9 (45)	11 (55)	30.727
91	Chromoblastomycosis	4 (0.05)	3 (100)		40.25
92	Cyst	1 (0.01)			26
93	Miliaria	3 (0.04)	1 (33.33)	2 (66.67)	15.667
94	Rhinophyma	3 (0.04)		1 (100)	40.333
95	Venus Ulcer	1 (0.01)	1 (100)		30
96	Fixed drug eruption	18 (0.22)	12 (75)	4 (25)	21.167
97	Melanoma	2 (0.02)	1 (50)	1 (50)	70
98	Pityriasis Rotunda	1 (0.01)	1 (100)		16
99	Tinea Barbae	4 (0.05)	4 (100)		36.5
100	Ashy Dermatitis	3 (0.04)	1 (33.33)	2 (66.67)	26.667
101	Pompholyx	2 (0.02)		2 (100)	26
102	Dermatitis cruris pustulosa atrophicans	4 (0.05)	2 (50)	2 (50)	30.5

103	Ramsay Hunt syndrome	1 (0.01)		1 (100)	58
104	Milia	2 (0.02)	1 (50)	1 (50)	21
105	Postherpetic neuralgia	1 (0.01)		1 (100)	54
106	Monkey-pox	9 (0.11)	7 (77.78)	2 (22.22)	31.111
107	Adnexal tumor	1 (0.01)	1 (100)		21
108	Linear verrulated epidermal nevus	1 (0.01)	1 (100)		20
109	Hand Dermatitis	18 (0.22)	7 (38.89)	11 (61.11)	24.889
110	Sarcoptes	1 (0.01)	1 (100)		27
111	Onchocerciasis	21 (0.25)	17 (80.95)	4 (19.05)	34
112	Folliculitis Decalvas	4 (0.05)	1 (25)	3 (75)	23.5
113	Cow Pox	1 (0.01)	1 (100)		40
114	Pyogenic granuloma	5 (0.06)	3 (60)	2 (40)	33.8
115	Varicose vein	2 (0.02)	1 (50)	1 (50)	26.5
116	Lipoma	4 (0.05)	2 (50)	2 (50)	27.25
117	Acanthosis Nigricans	2 (0.02)	1 (50)	1 (50)	21
118	Icthiosis	1 (0.01)		1 (100)	27
119	Keratosis Pillaris	3 (0.04)		3 (100)	18.667
Total		**8325**	**3722**	**3325**	

Appendix C: **Developed excel formula used for exploratory investigation of skin diseases**

Dsiseases	Total	Male	Female	Individual_Mean	Mean - total	Aprroximate_Age
					0	0
					0	0
	18	6	8	43.75	0	0
					787.5	788
					0	0
					0	0
					0	0
					0	0

Total	Male	Female	M		Male %	F	Female %	Total
487	271	216	0.5564681724846	55.6468172484	55.65	0.443531827515	44.3531827515	100
33	10	23	0.3030303030303030	30.3030303030	30.3	0.696969696969	69.6969696969	100
425	124	301	0.2917647058823529	29.1764705882	29.18	0.708235294117	70.8235294117	100
256	132	124	0.515625	51.5625	51.56	0.484375	48.4375	100
3	1	2	0.3333333333333333	33.3333333333	33.33	0.666666666666	66.6666666666	100
14	11	3	0.7857142857142857	78.5714285714	78.57	0.214285714285	21.4285714285	100
381	211	170	0.5538057742782152	55.3805774278	55.38	0.446194225721	44.6194225721	100
32	13	19	0.40625	40.625	40.63	0.59375	59.375	59.38
193	117	76	0.6062176165803111	60.6217616580	60.62	0.393782383419	39.3782383419	39.38
64	18	46	0.28125	28.125	28.13	0.71875	71.875	71.88
443	275	168	0.6207674943566591	62.0767494356	62.08	0.379232505643	37.9232505643	37.92
120	48	72	0.4	40	40	0.6	60	60
429	294	135	0.6853146853146853	68.5314685314	68.53	0.314685314685	31.4685314685	31.47
79	39	40	0.4936708860759494	49.3670886075	49.37	0.506329113924	50.6329113924	50.63
511	377	134	0.7254901960784314	72.5490196078	72.55	0.274509803921	27.4509803921	27.45
192	104	88	0.5520833333333333	55.2083333333	55.21	0.447916666666	44.7916666666	44.79
347	199	148	0.5734870317002882	57.3487031700	57.35	0.426512968299	42.6512968299	42.65
43	29	13	0.6976761904761905	69.7676190476	69.77	0.302323809523	30.2323809523	30.23
142	65	77	0.4577464788732394	45.7746478873	45.77	0.542253521126	54.2253521126	54.23
177	97	80	0.5480225988700565	54.8022598870	54.8	0.451977401129	45.1977401129	45.2
105	46	59	0.4380952380952381	43.8095238095	43.81	0.561904761904	56.1904761904	56.19
135	63	72	0.4666666666666667	46.6666666666	46.67	0.533333333333	53.3333333333	53.33
0			#NUM!	#NUM!	#NUM!	#NUM!	#NUM!	#NUM!
78	52	26	0.6666666666666667	66.6666666666	66.67	0.333333333333	33.3333333333	33.33
63	23	40	0.3650793650793651	36.5079365079	36.51	0.634920634920	63.4920634920	63.49
6	2	4	0.3333333333333333	33.3333333333	33.33	0.666666666666	66.6666666666	66.67
29	18	11	0.6206896551724138	62.0689655172	62.07	0.379310344827	37.9310344827	37.93
4	3	1	0.75	75	75	0.25	25	25
0			#NUM!	#NUM!	#NUM!	#NUM!	#NUM!	#NUM!
28	13	15	0.4642857142857143	46.4285714285	46.43	0.535714285714	53.5714285714	53.57
1	1		1	100	100	0	0	0
1		1	0	0	0	1	100	100
14	6	8	0.4285714285714286	42.8571428571	42.86	0.571428571428	57.1428571428	57.14
131	59	72	0.4503816793893130	45.0381679389	45.04	0.549618320610	54.9618320610	54.96
46	18	28	0.3913043478260870	39.1304347826	39.13	0.608695652173	60.8695652173	60.87
28	17	11	0.6071428571428571	60.7142857142	60.71	0.392857142857	39.2857142857	39.29
354	213	141	0.6016949152542373	60.1694915254	60.17	0.398305084745	39.8305084745	39.83
75	39	45	0.5866666666666667	58.6666666666	58.67	0.413333333333	41.3333333333	41.33
1	1		1	100	100	0	0	0
31	21	8	0.7241379310344828	72.4137931034	72.41	0.275862068965	27.5862068965	27.59
57	23	34	0.4035087719298246	40.3508771929	40.35	0.596491228070	59.6491228070	59.65
49	25	24	0.5102040816326531	51.0204081632	51.02	0.489795918367	48.9795918367	48.98
83	46	37	0.5542168674698795	55.4216867469	55.42	0.445783132530	44.5783132530	44.58
140	38	102	0.2714285714285714	27.1428571428	27.14	0.728571428571	72.8571428571	72.86
95	60	35	0.6315789473684211	63.1578947368	63.16	0.368421052631	36.8421052631	36.84
124	62	62	0.5	50	50	0.5	50	50
8	1	7	0.125	12.5	12.5	0.875	87.5	87.5
14	11	3	0.7857142857142857	78.5714285714	78.57	0.214285714285	21.4285714285	21.43
0			#NUM!	#NUM!	#NUM!	#NUM!	#NUM!	#NUM!
42	20	22	0.4761904761904762	47.6190476190	47.62	0.523809523809	52.3809523809	52.38
36	16	20	0.4444444444444444	44.4444444444	44.44	0.555555555555	55.5555555555	55.56
46	30	16	0.6521739130434783	65.2173913043	65.22	0.347826086956	34.7826086956	34.78
3		3	0	0	0	1	100	100
66	36	30	0.5454545454545455	54.5454545454	54.55	0.454545454545	45.4545454545	45.45
63	37	26	0.5873015873015873	58.7301587301	58.73	0.412698412698	41.2698412698	41.27
97	58	39	0.5979381443298969	59.7402597402	59.74	0.402597402597	40.2597402597	40.26
20	11	9	0.55	55	55	0.45	45	45
71	41	30	0.5774647887323944	57.7464788732	57.75	0.422535211267	42.2535211267	42.25
100	53	47	0.53	53	53	0.47	47	47
1	1		1	100	100	0	0	0
0			#NUM!	#NUM!	#NUM!	#NUM!	#NUM!	#NUM!
17	9	8	0.5294117647058824	52.9411764705	52.94	0.470588235294	47.0588235294	47.06
11	1	10	0.0909090909090909	9.0909090909	9.09	0.909090909090	90.9090909090	90.91
22	11	11	0.5	50	50	0.5	50	50
27	10	17	0.3703703703703704	37.0370370370	37.04	0.629629629629	62.9629629629	62.96
19		19	0	0	0	1	100	100
9	6	3	0.6666666666666667	66.6666666666	66.67	0.333333333333	33.3333333333	33.33
9	4	5	0.4444444444444444	44.4444444444	44.44	0.555555555555	55.5555555555	55.56
10	1	9	0.9	90	90	0.1	10	10
0			#NUM!	#NUM!	#NUM!	#NUM!	#NUM!	#NUM!
24	14	10	0.5833333333333333	58.3333333333	58.33	0.416666666666	41.6666666666	41.67
14	8	6	0.4285714285714286	42.8571428571	42.86	0.571428571428	57.1428571428	57.14
13	10	3	0.7692307692307692	76.9230769230	76.92	0.230769230769	23.0769230769	23.08
9	5	4	0.5555555555555556	55.5555555555	55.56	0.444444444444	44.4444444444	44.44
23	13	10	0.5652173913043478	56.5217391304	56.52	0.434782608695	43.4782608695	43.48
17	7	10	0.4117647058823529	41.1764705882	41.18	0.588235294117	58.8235294117	58.82
8	5	3	0.625	62.5	62.5	0.375	37.5	37.5
34	21	13	0.6176470588235294	61.7647058823	61.76	0.382352941176	38.2352941176	38.24
2	2		1	100	100	0	0	0
6	2	4	0.3333333333333333	33.3333333333	33.33	0.666666666666	66.6666666666	66.67
32	18	14	0.5625	56.25	56.25	0.4375	43.75	43.75
5	1	4	0.2	20	20	0.8	80	80
164	90	74	0.5487804878048780	54.8780487804	54.88	0.451219512195	45.1219512195	45.12
1	1		1	100	100	0	0	0
276	147	129	0.5326086956521739	53.2608695652	53.26	0.467391304347	46.7391304347	46.74
6	3	3	0.5	50	50	0.5	50	50
1	1		1	100	100	0	0	0
1	1		1	100	100	0	0	0
9	7	2	0.7777777777777778	77.7777777777	77.78	0.222222222222	22.2222222222	22.22
20	9	11	0.45	45	45	0.55	55	55
3	3		1	100	100	0	0	0
0			#NUM!	#NUM!	#NUM!	#NUM!	#NUM!	#NUM!
3	1	2	0.3333333333333333	33.3333333333	33.33	0.666666666666	66.6666666666	66.67
1	1		0	0	0	1	100	100
1	1		1	100	100	0	0	0
16	12	4	0.75	75	75	0.25	25	25
2	1	1	0.5	50	50	0.5	50	50
1	1		1	100	100	0	0	0
1	1		1	100	100	0	0	0
3	1	2	0.3333333333333333	33.3333333333	33.33	0.666666666666	66.6666666666	66.67
2		2	0	0	0	1	100	100
4	2	2	0.5	50	50	0.5	50	50
2	1	1	0.5	50	50	0.5	50	50
1	1		1	100	100	0	0	0
2	1	1	0.5	50	50	0.5	50	50
1	1		1	100	100	0	0	0
9	7	2	0.7777777777777778	77.7777777777	77.78	0.222222222222	22.2222222222	22.22
1	1		1	100	100	0	0	0
1	1		1	100	100	0	0	0
18	7	11	0.3888888888888889	38.8888888888	38.89	0.611111111111	61.1111111111	61.11
1	1		1	100	100	0	0	0
21	17	4	0.8095238095238095	80.9523809523	80.95	0.190476190476	19.0476190476	19.05
4	1	3	0.25	25	25	0.75	75	75
1	1		1	100	100	0	0	0
5	3	2	0.6	60	60	0.4	40	40
1	1		0.5	50	50	0.5	50	50
4	2	2	0.5	50	50	0.5	50	50
2	1	1	0.5	50	50	0.5	50	50
1	1		1	100	100	0	0	0
3		3	0	0	0	1	100	100